## SECTION III. TASK 3. COMPREHENSIVE MODEL DEVELOPMENT AND EVALUATION

### Objectives

The objective of this task is to integrate advanced chemistry and physics submodels into a comprehensive two-dimensional model of entrained-flow reactors (PCGC-2) and to evaluate the model by comparing with data from well-documented experiments. Approaches for the comprehensive modeling of fixed-bed reactors will also be reviewed and evaluated and an initial framework for a comprehensive fixed-bed code will be employed after submission of a detailed test plan (Subtask 3.b).

### Task Outline

This task will be performed in three subtasks. The first covering the full 60 months of the program will be devoted to the development of the entrained-bed code. The second subtask for fixed-bed reactors will be divided into two parts. The first part of 12 months will be devoted to reviewing the state-of-the-art in fixed-bed reactors. This will lead to the development of the research plan for fixed-bed reactors. After approval of the research plan, the code development would occupy the remaining 45 months of the program. The third subtask to generalize the entrained-bed code to fuels other than dry pulverized coal would be performed during the last 24 months of the program.

## III.A. SUBTASK 3.A. - INTEGRATION OF ADVANCED SUBMODELS INTO ENTRAINED-FLOW CODE, WITH EVALUATION AND DOCUMENTATION

Senior Investigators - B. Scott Brewster and L. Douglas Smoot
Brigham Young University
Provo, UT 84602
(801) 378-6240 and 4326

Graduate Research Assistant - Michael L. Hobbs

### Objectives

The objectives of this subtask are 1) to improve an existing 2-dimensional code for entrained coal combustion/gasification to be more generally applicable to a variety of coals by incorporating advanced coal chemistry submodels, advanced numerical methods, and an advanced pollutant submodel for both sulfur and nitrogen species, and 2) to validate the advanced submodels in the comprehensive code. The comprehensive code into which the advanced submodels are to be incorporated is PCGC-2 (Pulverized Coal Gasification and Combustion-2 dimensional).

### Accomplishments

Work on this subtask is being accomplished under five components: 1) Evaluation and incorporation of coal reaction submodels into the comprehensive code, 2) incorporation of improved numerical solution methods, 3) incorporation of the $SO_x$-$NO_x$ submodel being developed under subtask 2.g, 4) implementation of the code on computers, and 5) code evaluation. Progress during the second year is described below for each of these components.

#### Component 1 - Evaluation and Incorporation of Coal Reaction Submodels

This component is aimed at incorporating advanced coal reaction submodels into PCGC-2. During the last year, modifications were made in PCGC-2 to investigate the effects of variable coal offgas composition with two solids progress variables independently tracking separate coal offgas components. The FG/DVC submodel was also incorporated into PCGC-2. Development of a laminar option was initiated for validating the FG/DVC submodel without the complicating effects of turbulence.

Effects of Variable Coal Offgas Composition - During the first year, a three-pronged approach was conceptualized for integrating the FG/DVC submodel into PCGC-2. The approach consists of three methods and is described in the 1st Annual Report (Solomon et al., 1987). The first method is referred to as the Single Solids Progress Variable (SSPV) method and uses a single progress variable to track the evolution and mixing of coal offgas (consisting of all material originating from the coal) throughout the reactor. Progress variables which track material originating from the solid phase are referred to as "solids progress variables." The SSPV method does not account for variability in the offgas composition with extent of burnout and is the method currently employed in PCGC-2 (Smoot et al., 1988). In the Multiple Solids Progress Variable (MSPV) method, the offgas is divided into multiple components, each component being tracked independently with its own progress variable. With two or more solids progress variables, the total offgas composition may vary with extent of

burnout. The additional progress variables lead to expensive computer solutions, however, and must be carefully justified. It is estimated that each additional fluctuating progress variable will increase the computational burden by an order of magnitude. A third method for integrating the FG/DVC submodel, the Statistical Gas Dispersion (SGD) method, is based on a statistical Lagrangian description of the gas and has the potential of accounting for variability in offgas composition without significantly increasing the computational burden. However, the SGD method is a radically new approach, and the MSPV method is being considered first, since it is an extension of the current method.

During the past year, a simple procedure was devised and implemented to test the MSPV method and investigate the effects of allowing for variability in offgas composition on comprehensive code predictions without making extensive modifications in the code. PCGC-2 currently has two progress variables, one for tracking the mixing of the primary and secondary gas streams, and the other for tracking the mixing of the coal offgas with the total inlet gas. Two test cases were prepared where, in each case, the primary and secondary gas streams were identical in composition and enthalpy, thus obviating the need for a progress variable to track the mixing of these streams. One case was a swirling, slightly fuel-lean combustion case, and the other was a non-swirling, oxygen-blown, gasification case. Simple modifications were made in PCGC-2 to allow the coal gas mixture fraction (used normally to track the coal offgas mixing) to track the mixing of the coal volatiles, and the inlet gas mixture fraction (used normally to track the mixing of primary and secondary) to track the mixing of the carbon evolved during heterogeneous oxidation of the residual char. The results for these two cases were presented in the 6$^{th}$ Quarterly Progress Report (Solomon et al., 1988) and in two papers presented and published during the past year (Brewster and Smoot, 1988; Brewster et al., 1988).

The results for the combustion case clearly illustrate the importance of accounting for variability in coal offgas composition, as shown in Figure III.A-1. The gas temperature fields for the SSPV and MSPV methods are both characterized by a high-temperature, stoichiometric ridge surrounding a low-temperature, fuel-rich zone where the particles are devolatilizing. This structure is evident in both the surface and contour plots and is typical of combustors that are slightly fuel-lean. In the case of the MSPV method, where volatiles and char oxidation offgas are tracked separately, and overall offgas composition is thus allowed to vary, the fuel-rich zone is significantly smaller and less fuel-rich. The reason for this difference is that the early offgas contains all of the non-carbon elements (including oxygen) while the late offgas is only carbon (from char oxidation). This difference in flame structure further manifests itself through significant differences in gas composition and burnout. Details may be found in the 6$^{th}$ Quarterly Progress Report (Solomon et al., 1988).

The differences between the SSPV and MSPV methods are not as striking for the gasification case. Temperature surface plots for this case are shown in Figure III.A-2. As shown, the reaction is very rapid, achieving complete burnout in a very short region of the reactor, with the temperature profile essentially flat thereafter. The process is fuel-rich overall, and there is no fuel-rich depression surrounded by a high-temperature stoichiometric ridge, as in the slightly fuel-lean combustion case. Since both devolatilization and char oxidation rapidly proceed to completion in a short, initial region of the

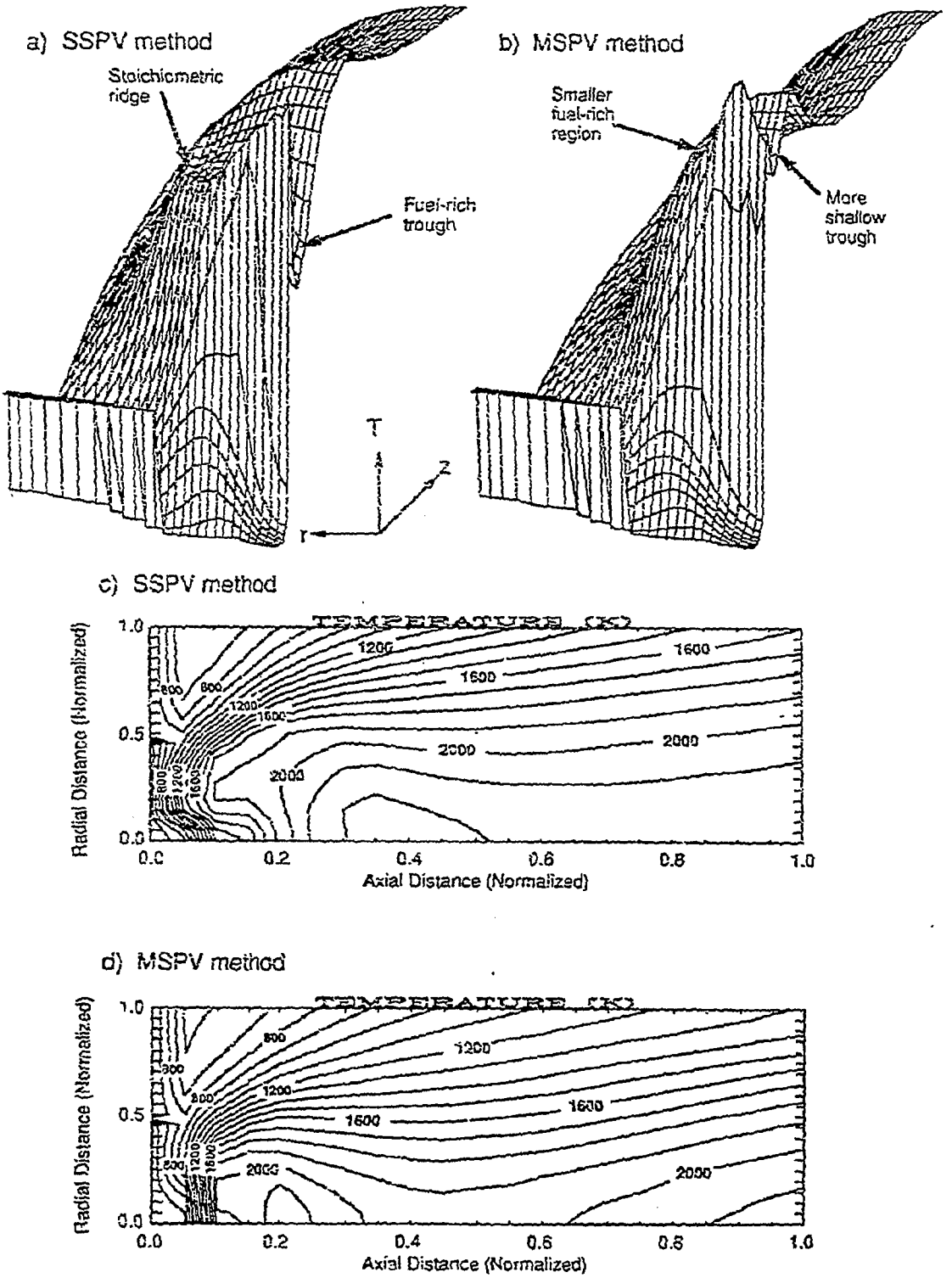


Figure III.A-1. Gas temperature isotherms and surface plots for swirled combustion case.

a) SSPV method

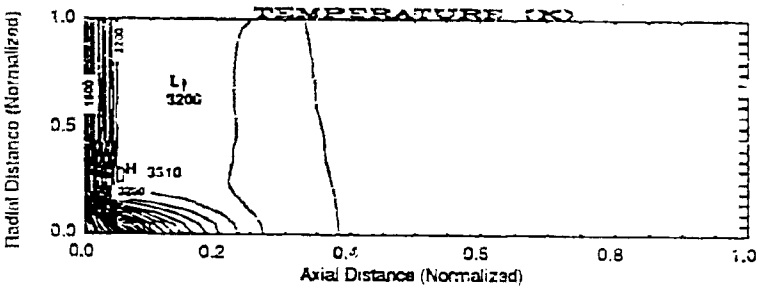


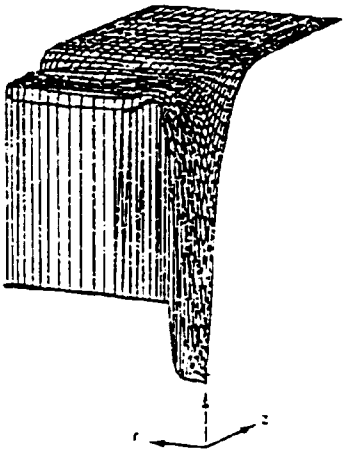

b) MSPV method (Char offgas and volatiles tracked separately)

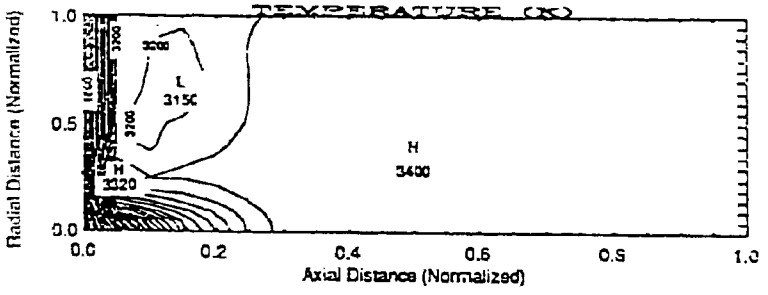


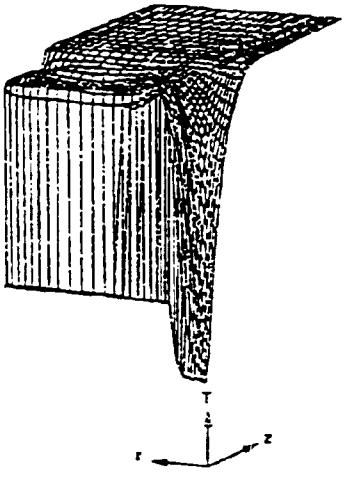

Figure III.A-2. Gas temperature isotherms and surface plots for gasification case.

reactor, rather than being distributed throughout the reactor, letting volatiles and char offgas evolve at different rates does not make a significant difference compared with assuming they evolve at the same rate. The reason for the rapid reaction in this case is the high gas temperature (over 3000 K). This calculation was performed for an oxygen-blown case assuming no external heat loss. If external heat loss were taken into account, the gas temperature would be lower, the reaction would be distributed over a somewhat larger region of the reactor, and the effects of allowing volatiles and char offgas to evolve at different rates would be more important.

The division of the offgas into volatiles and char offgas seems natural since devolatilization and oxidation are independent processes. Actually, the division into two or any number of components for tracking purposes is arbitrary, as long as the composition of each component is fully defined and constant. One alternative is to independently track individual chemical elements, such as carbon, hydrogen, and oxygen, or groups of elements that evolve at similar rates. In this approach, no consideration is given to the chemical species containing the element when it evolves from the coal or to the subprocess that produced it. Only the rate of evolution as a function of burnout need be known. Hydrogen, for example evolves earlier than other elements (Smoot and Smith, 1985). It therefore seems logical to divide the offgas into hydrogen offgas and offgas containing all other elements in the coal. This approach was implemented in PCGC-2 and tested with the gasification case. However, the results were similar to those shown in Figure III.A-2, i.e. the effects of allowing hydrogen to evolve independently at a higher rate than the other elements were negligible. Although the element approach for the MSPV method was not tested with the combustion case, the results would probably be similar to those shown in Figure III.A-1.

The phenomenological approach (e.g. independently tracking products of separate subprocesses) may be more satisfying intuitively, but could ultimately require an additional progress variable for each of the nineteen light gas species in the FG/DVC submodel and for each heterogeneous reaction with the char. The elemental approach, on the other hand, limits the total number of progress variables to the number of elements in the coal, but may suffer from the disadvantage of being more empirical and less general. From the standpoint of the expected increase in required computing power, it is felt that a maximum of two or three progress variables for the coal offgas is a reasonable number to consider, however the number required for adequate modeling purposes and how they should be defined are still being considered.

Integration of FG/DVC Submodel into PCGC-2 - The FG/DVC submodel was integrated into PCGC-2 as an option that can be selected in the main input file. The original integration was described in the 5th Quarterly Progress Report under Subtask 4.a (Solomon et al., 1987). The original submodel integration increased the required computer time for the comprehensive code simulation by a factor of approximately four, but only a modest increase was achieved by decreasing the coal polymer sample size by a factor of 3 or 4, and decreasing the frequency of the calls to the DVC subroutine to every 10 degrees change in particle temperature at temperatures greater than 500 degrees Centigrade. Below 500 C, the particles are assumed to be inert. The interface between the two codes and the purposes of the FG/DVC subroutines were described in the 7th Quarterly Progress Report (Solomon et al., 1988). A partial listing of the key

Fortran variables in the FG/DVC submodel has been prepared and is included in the appendix.

Laminar Option - One of the more important tasks of this study is to validate the comprehensive code with advanced coal reaction submodels by comparing code predictions with discriminating experimental data. Unfortunately, such data are limited for turbulent reactors and also complicate the evaluation of the FG/DVC submodel through turbulence effects. Therefore, the validation of the integrated FG/DVC submodel with laminar data is viewed as being critical to the total validation effort, and laminar data being obtained by AFR in their transparent wall reactor (TWR) under Subtask 2.c of this study will be an important element in this effort. The validation will be performed under Component 5 of this subtask, but development of a laminar option in the comprehensive code is discussed here, because of its close link with submodel integration.

Previously, the general capability to simulate laminar reactors or reactors in the upflow configuration did not exist in PCGC-2. The option to simulate the upflow configuration was added by including a flag in the main datafile that sets the sign on the gravity term in the particle equation of motion. The option to simulate laminar reactors is being added by turning off all turbulence calculations and calculating molecular transport parameters (viscosity, thermal conductivity, and diffusivity) as functions of local composition and temperature. Free convection, buoyancy forces, and the effects of the particles on the transport properties of the gas, are neglected. A sample main input file for a laminar upflow simulation is shown in Table III.A-1. Explanations for the data entries in this file can be found in the PCGC-2 User s Manual (Smoot et al., 1988) with the following exceptions: All of the data entries on lines 15, 16, 81 through 112, and 123 through 126, have been added as a part of the modifications to test the MSPV method, integrate the FG/DVC submodel, and add the laminar and upflow options. These new data entries are summarized in Table III.A-2. The entries on lines 123 through 125 specify the names of the coal data file, functional group kinetics data file, and polymer data file.

The new and modified data files associated with the modification and integration of the FG/DVC submodel into PCGC-2 are described in Table III.A-3. The main input datafile (PCGCIN) was modified to include logical data for controlling the SSPV/MSPV methods and selecting the FG/DVC submodel, character data for specifying the flow configuration (up-flow or down-flow) and file names needed for the FG/DVC submodel, and data for calculating the enthalpy of each functional group and specifying the coal polymer sample size. An output file was added for summarizing results from the FG/DVC submodel. Three additional input files are required by the FG/DVC submodel for specifying the coal composition, functional group rate parameters, and coal polymer structure. The names of these data files are arbitrary, since they are specified in the main datafile.

The laminar option in PCGC-2 is being used to simulate the transparent wall reactor for combustion of Montana Rosebud coal as described under Subtask 2.c in the First Annual Report (Solomon et al., 1987). Key parameters for this simulation are shown in Table III.A-4. The generalized geometry feature of PCGC-2 as described in the Revised User's Manual (Smoot et al., 1988) was used to simulate the geometry of the injection nozzle. The additional inlet feature

## Table III.A-1
## SAMPLE MAIN INPUT DATA FILE FOR PCGC-2

```
Line
No.   Main input file data:

1       7,                                          !NSAY..(SAY(I),I=1,NSAY) follows:
2       Laminar flow case, simulating transparent wall reactor.
3       Constant laminar viscosity, input turbulence intensity is zero.
4       Primary stream is cold air, secondary stream is hot air.
5       Primary stream contains Montana Rosebud coal.
6       FG/DVC model used.
7       Grid modified to include coal injection nozzle.
8       Use Solomon single-rate kinetics instead of FGDVC.
9      T     T     T     F     F                    !INRST,INCALF,INCREK,INCALH,INCALG
10     T     T     F     T     F                    !IPSICT,INPRST,INEACH,INCLET,INCLGE
11     T     F     F     F     T                    !INCALN,INCURF,LEULP,INTFRZ,INISMP
12     F     F     F     F     F                    !INCNOX,POLLUT,INQRL,INCSWP,INCSWS
13     T     F     F     T     F                    !INNOZZ,INFSOU,LTBUG,GRDOUT,INPROG
14     F     T     T     F     F                    !INCFP,INRAD,INRDGD,INTRUS,MAGHJER
15     F     F     F     T                          !INETA2,HTRACK,FGDVC,LAMINAR
16    up-fired                                     !config
17     0.700,0.700,0.700,0.800,                    !URFU,URFV,URFW,URFH
18     0.700,0.700,0.700,0.700,0.700,              !URFE,URFK,URFF,URFG,URFVIS
19     0.500,0.700,0.700,1.000,1.000,1.000,        !URFDEN,URFETA,URFGET,URFNJ,URFPP,URFP
20      1.85E-3, 10.0E-2, 21.5E-2,                  !DIAP,DIAS,DIACH
21        3.255814, 0.002025,                       !NDIA(real),THICK
22      1000, 999,  50,                            !MAXIT,INDPRI,INDRST
23        5,  17,  40,                              !NJINP,NJINS,NIWOQ
24      100.000, 1.100,25, 1.100, 0.900,            !AL1,EPSX,NL,EPSI,EPSD
25      -360.0     ,  15.0       , 0.00000E+00,    !HRMIN,HRMAX,HLOSS
26                 4,  35.000     , 4.00000E-02,    !NIINQ,QHA,QLX
27            350.00,      350.00,      0.00,       !TBN,TBW,TBE
28      1.79000E-05,  101325.,                      !VISCOS,PRES
29       0.01000000,  0.10000000,                   !SORMAX,SORMIN
30    INLET 1                                      !(Cold carrier air)
31      4.41168E-6, 1.000, 0.000,  0.0,             !FLOW,FFLOW,SWIRLN,TINFLO
32    INLET 2                                      !(Hot air)
33      3.34313E-03, 0.000, 0.000,  0.0,            !FLOW,FFLOW,SWIRLN,TINFLO
```

Table III.A-1 (continued)
SAMPLE MAIN INPUT DATA FILE FOR PCGC-2

```
Line
No.   Main input file data:

34    INLET 3                                          !(Cold room air)
35      0.0466981, 1.000, 0.000,  0.0,                 !FLOW,FFLOW,SWIRLN,TINFLO
36                                                     !                        (Blank line)
37    ELEMENTS
38    THERMO                                           !The react. sect. is formatted
39    REACTANTS 1
40        300.000                                      !TMP (unformatted)
41    O 2.        0.        0.        0.      O2          0.21000M         G
42    N 2.        0.        0.        0.      N2          0.79000M         G
43                                                     !                        (Blank line)
44    REACTANTS 2
45        1123.000                                      !TMP (unformatted)
46    O 2.        0.        0.        0.      O2          0.21000M         G
47    N 2.        0.        0.        0.      N2          0.79000M         G
48                                                     !                        (Blank line)
49     10, 5,                                          !NSL,NPS
50      4.9112054,1340.000,                              !PLOADP,PDEN
51    0.0000,0.0000,0.0000,0.0000,0.0000,              !YPS(ISL),ISL = 1,5
52    0.0000,0.0000,0.0000,0.0000,0.0000,              !YPS(ISL),ISL = 6,NSL
53    1.0000,1.0000,1.0000,1.0000,1.0000,              !UPLAG(IPS),IPS = 1,NPS
54    0.0000,0.0000,0.0000,0.0000,0.0000,              !SPRANG(ISL),ISL = 1,5
55    0.0000,0.0000,0.0000,0.0000,0.0000,              !SPRANG(ISL),ISL = 6,NSL
56    1.0000,1.0000,1.0000,1.0000,1.0000,              !TLAG(IPS),IPS = 1,NPS
57     45.0E-06,52.5E-06,60.0E-06,                     !PD(IPS),IPS = 1,3
58     67.5E-06,75.0E-06,                              !PD(IPS),IPS = 4,NPS
59    0.2000,0.2000,0.2000,0.2000,0.2000,              !PMF(IPS),IPS = 1,NPS
60    F    F    T    F    F                           !LDEBUG,LYPS,LPARTP,LPARTS,LPBOTH
61    T    T    T    F                                !LSPM,LSPU,LSPV,LSPH
62    0.9500,0.0200,                                   !YPSH,YPSL
63     10, 10,  3,                                     !MAXITP,MINITP,IGASV
64    0.350,0.350,0.350,0.350,0.350,                   !PRK(IPS),IPS = 1,NPS
65     1                                               !NCARD...COMENT(I),I=1,NCARD follows:
66                    All Particles have the same Properties
```

## Table III.A-1 (continued)
## SAMPLE MAIN INPUT DATA FILE FOR PCGC-2

```
Line
No.   Main input file data:

67     T                                                !INCOAL
68      1   1   5   1   0   0                           !NCRXN,NHRXN,NPROP,IEUCK,KEQ,NSHRNK
69      1.000E-02, 1.000E-06, 0.000    ,0.500           !DELTPJ,DELRRJ,GAMMA,URFPM
70       1.0000                                         !XI(J)
71      0.00000E+00, 0.00000E+00,-1.50400E+07,          !QHC(J),HH0(J),HA0(J)
72     -1.58800E+07,  373.15    ,                       !HW0(J),TNBP
73      0.84900    , 0.00000E+00, 0.15100,              !OMEGAC(J),OMEGAH(J),OMEGAA(J)
74      0.00000E+00,                                    !OMEGAW(J)
75      4.28E+14, 2.285E+08, 0.40000    , !AMJ(J,M),EMJ(J,M),YY(J,M)
76      0.00000E+00,                                    !HGV(J,M)
77       10.400    , 9.31000E+07,  1.0000    ,         !AL(J,L),EL(J,L),EMM(J,L)
78       0000.0    , 0.00000E+00, 0.00000E+00,         !CCPC(J)
79       0000.0    , 0.00000E+00, 0.00000E+00,         !CCPH(J)
80        000.0    , 0.00000E+00, 0.00000E+00,         !CCPA(J)
81     1.980E+1  7.344E-2 -5.602E-5  1.715E-8 -3.938E+5  44.010  !CPCOEF(01,J),HFG0(01),MW(01) 1-CO2-LOOSE
82     2.731E+1  2.383E-2  1.707E-5 -1.185E-8 -4.572E+4  17.031  !CPCOEF(02,J),HFG0(02),MW(02) 2-NH3
83     1.980E+1  7.344E-2 -5.602E-5  1.715E-8 -3.938E+5  44.010  !CPCOEF(03,J),HFG0(03),MW(03) 3-CO2-TIGHT
84     3.087E+1 -1.285E-2  2.789E-5 -1.272E-8 -1.106E+5  28.010  !CPCOEF(04,J),HFG0(04),MW(04) 4-ETHER-CO-TIGHT
85     2.714E+1  9.274E-3 -1.381E-5  7.645E-9  0.000E+0   2.016  !CPCOEF(05,J),HFG0(05),MW(05) 5-AROMATIC HYDROGEN
86     2.816E+1  6.062E-2 -4.961E-5  1.815E-8  1.306E+5  27.026  !CPCOEF(06,J),HFG0(06),MW(06) 6-HCN-TIGHT
87     2.816E+1  6.062E-2 -4.961E-5  1.815E-8  1.306E+5  27.026  !CPCOEF(07,J),HFG0(07),MW(07) 7-HCN-LOOSE
88     3.224E+1  1.924E-3  1.055E-5 -3.596E-9 -2.420E+5  18.015  !CPCOEF(08,J),HFG0(08),MW(08) 8-H2O-TIGHT
89     2.115E+1  7.092E-2  2.587E-5 -2.852E-8 -2.013E+5  32.042  !CPCOEF(09,J),HFG0(09),MW(09) 9-METHANOL
90     3.087E+1 -1.285E-2  2.789E-5 -1.272E-8 -1.106E+5  28.010  !CPCOEF(10,J),HFG0(10),MW(10) 10-CO-EXTRA TIGHT
91     3.224E+1  1.924E-3  1.055E-5 -3.596E-9 -2.420E+5  18.015  !CPCOEF(11,J),HFG0(11),MW(11) 11-H20-LOOSE
92     1.980E+1  7.344E-2 -5.602E-5  1.715E-8 -3.938E+5  44.010  !CPCOEF(12,J),HFG0(12),MW(12) 12-CO2-EXTRA-LOOSE
93     3.087E+1 -1.285E-2  2.789E-5 -1.272E-8 -1.106E+5  28.010  !CPCOEF(13,J),HFG0(13),MW(13) 13-CO-LOOSE
94     1.925E+1  5.213E-2  1.197E-5 -1.132E-8 -7.490E+4  16.043  !CPCOEF(14,J),HFG0(14),MW(14) 14-CH4-EXTRA LOOSE
95     0.000E+0  0.000E+0  0.000E+0  0.000E+0  0.000E+0  0.00001 !CPCOEF(15,J), ----- EMPTY -- 15-
96     3.806E+0  1.566E-1 -8.348E-5  1.755E-8  5.234E+4  28.054  !CPCOEF(16,J),HFG0(16),MW(16) 16-C2H4
97     3.710E+0  2.345E-1 -1.160E-4  2.205E-8  2.043E+4  42.081  !CPCOEF(17,J),HFG0(17),MW(17) 17-C3H6
98     -1.746E0  5.309E-1 -2.903E-4  6.054E-8 -4.170E+4  84.163  !CPCOEF(18,J),HFG0(18),MW(18) 18-OLEFINS
99     5.409E+0  1.781E-1 -6.938E-5  8.713E-9 -8.474E+4  30.070  !CPCOEF(19,J),HFG0(19),MW(19) 19-C2H6
```

Table III.A-1 (continued)
SAMPLE MAIN INPUT DATA FILE FOR PCGC-2

```
Line
No.   Main input file data:

100    -4.224E0  3.063E-1 -1.586E-4  3.215E-8 -1.039E+5  44.094  !CPCOEF(20,J),HFG0(20),MW(20) 20-C3H8
101    -4.413E0  5.820E-1 -3.119E-4  6.494E-8 -1.673E+5  86.178  !CPCOEF(21,J),HFG0(21),MW(21) 21-PARAFFINS
102    1.925E+1  5.213E-2  1.197E-5 -1.132E-8 -7.490E+4  16.043  !CPCOEF(22,J),HFG0(22),MW(22) 22-CH4-LOOSE
103    1.925E+1  5.213E-2  1.197E-5 -1.132E-8 -7.490E+4  16.043  !CPCOEF(23,J),HFG0(23),MW(23) 23-CH4-TIGHT
104    -4.413E0  5.820E-1 -3.119E-4  6.494E-8 -1.673E+5  86.178  !CPCOEF(24,J),HFG0(24),MW(24) 24-C-ALIPHATIC
105    -4.413E0  5.820E-1 -3.119E-4  6.494E-8 -1.673E+5  86.178  !CPCOEF(25,J),HFG0(25),MW(25) 25-H-ALIPHATIC
106    2.682E+1  7.178E-2 -5.007E-5  1.412E-8  2.269E+5  26.038  !CPCOEF(26,J),HFG0(26),MW(26) 26-C2H2
107    0.000E+0  0.000E+0  0.000E+0  0.000E+0  0.000E+0  12.011  !CPCOEF(27,J),HFG0(27),MW(27) 27-CHAR(CARBON)
108    0.000E+0  0.000E+0  0.000E+0  0.000E+0  0.000E+0  0.00001 !CPCOEF(28,J), --- 28-TAR (DATA ELSEWHERE)
109    0.000E+0  0.000E+0  0.000E+0  0.000E+0  0.000E+0  0.00001 !CPCOEF(29,J), --- EMPTY ---
110    0.000E+0  0.000E+0  0.000E+0  0.000E+0  0.000E+0  32.064  !CPCOEF(30,J), --- 30-INORG S
111    0.000E+0  0.000E+0  0.000E+0  0.000E+0  0.000E+0  0.00001 !CPCOEF(31,J), --- 31-MISSING
112    0.000E+0  0.000E+0  0.000E+0  0.000E+0  0.000E+0  0.00001 !CPCOEF(32,J), --- 32-ABSTRACTED
113     0.72400,    0.04900,      0.20300,        !(WIC(J,K) K = 1,3)
114     0.01200,    0.01200,                      !(WIC(J,K) K = 4,NLM)
115    H2O                                        !SLRCMP
116    O2                                         !OXYD(L),L = 1,NHRXN
117     2.00,                                     !PHIL(L) L = 1,NHRXN
118    T     T     T     ,  10                    !LDISO,LGASE,LEMCOR,MAXITR
119    0.9300,0.8600,0.8200,0.8200,0.8200,       !(QAB(IPS),IPS = 1,NPS)
120    0.3300,0.3100,0.3000,0.3000,0.3000,       !(QSC(IPS),IPS = 1,NPS)
121    0.1000,    0.00                           !EMW,TOUT
122    1.0000,0.0000                             !A0,AF
123   coal.rose                                  !Functional group composition datafile
124   fgkin                                      !Functional group kinetics datafile
125   polymr.wyodak                              !Coal polymer datafile
126   0.25,                                      !Coal polymer sample size scaling factor
```

Table III.A-2

NEW DATA ENTRIES IN MAIN INPUT FILE FOR PCGC-2

| Fortran Variable | Type | Units | Description and Usual Symbol |
|---|---|---|---|
| CONFIG | character*20 | - - | 'up-fired' selects the vertical, counter-gravity configuration. Anything else selects the vertical, co-gravity configuration. |
| CPCOEF(I,J) | real*4 | J mol-1 K-J | Heat capacity coefficients (J=1,4) for the $i^{th}$ functional group in the char. |
| FGDVC | logical | - - | .TRUE. will use the FGDVC submodel for devolatilization. |
| HFG0(I) | real*4 | J mol-1 | Heat of formation of the $I^{th}$ functional group. |
| HTRACK | logical | - - | .TRUE. will use inlet gas mixture fraction (f) to track hydrogen and coal gas mixture fraction ($\eta$) to track all other elements. .FALSE. will use inlet gas mixture fraction to track char offgas and coal gas mixture fraction to track volatiles. (INETA2 must be .TRUE. in both cases.) |
| INETA2 | logical | - - | .TRUE. will use two solids progress variables to track coal offgas. |
| LAMINAR | logical | - - | .TRUE. will turn off the turbulence submodel and calculate local viscosity and Prandtl number as functions of temperature and composition. |
| MW(I) | real*4 | kg kmol-1 | Molecular weight of the $I^{th}$ functional group. |
| SCALE | real*4 | - - | Scaling factor for the coal polymer sample size used in the DVC calculations. The initial nos. of oligomers (OLIGST), monomers (BEAD), hard bonds (FETHYL), crosslinks (FLINK), as specified in the coal polymer datafile get multiplied by SCALE. |

TABLE III.A-3

NEW OR MODIFIED FILES ASSOCIATED WITH PCGC-2 WITH THE INTEGRATED FG/DVC SUBMODEL

| Generic Name | Specific Name | Type | Description |
|---|---|---|---|
| FGOUT | 'runid'.fgo | Output | Output file for FG/DVC submodel. |
| PCGCIN | 'runid'.dat | Input | Main input file. Modified to include input data shown in Table III.A-2 and specification of coal, functional group kinetics, and polymer datafiles. A sample main input file is shown in Table III.A-1. |
| -- | As specified in main input file. | input | Coal data file. Contains functional group composition. |
| -- | As specified in main input file. | Input | Functional group kinetics data file. Contains pre-exponential factor, activation energy, and variance in activation energy for each functional group. |
| -- | As specified in main input file. | Input | Polymer data file. Contains information for generating the coal polymer structure in the DVC model. |

TABLE III.A-4

KEY INPUT DATA USED IN LAMINAR SIMULATION OF
TRANSPARENT WALL REACTOR FOR
COMBUSTION OF MONTANA ROSEBUD COAL

| Description | Value |
|---|---|
| Primary duct diameter | 1.0 mm |
| Nozzle inside diameter | 4.9 mm |
| Nozzle outside diameter | 5.9 mm |
| Distance that nozzle extends into the reactor | 5.7 mm |
| Carrier gas flowrate | 225 ml/min |
| Carrier gas temperature | 300 K |
| Input gas flowrate | 175 l/min |
| Input gas temperature | 1123 K |
| Secondary duct diameter | 10 cm |
| Coal feedrate | 1.3 g/min |
| Ash content (dry basis) | 15.1 wt. % |
| Nominal particle size | 45-75 microns |
| Reactor diameter | 21.5 cm |
| Total height of glass enclosure | 70 cm |
| Room air flowrate | $4.67 \times 10^{-2}$ kg/s |
| Room air temperature | 300 K |

was used to simulate the flow of room air inside the glass enclosure as described in the First Annual Report. Radial and axial grids were concentrated near the centerline and near the inlet of the of the reactor, respectively, to adequately resolve the flow near the nozzle. Radial grids were also concentrated in the region separating the hot inlet air and the cold room air.

Preliminary results are shown in Figures III.A-3 through 6. The particles do not disperse very much radially, as shown in Figure III.A-3. Fifty particle trajectories were calculated, for five particle sizes and ten starting locations. The particle size distribution was assumed to be uniform between the limits of 45 and 75 microns. Contour and surface plots of gas temperature are shown in Figure III.A-4. The step change in gas temperature from 1173 K to 300 K between the preheated inlet gas and the room air near the wall can be clearly seen at the front wall of the reactor. This step change is somewhat smoothed out at the exit due to radial dispersion, but the air temperature is still cool at the wall. High temperatures are seen only near the centerline at the inlet. The temperature goes through a sharp spike where the local gas mixture is stoichiometric, and then quickly drops as the available oxygen is consumed and the local gas becomes fuel-rich. A similar high-temperature spike is predicted in turbulent combustion, but it is broader. The sharpness of the spike in the laminar case is caused by the absence of turbulent transport.

The absence of oxygen in the region behind the initial temperature spike is shown in Figure III.A-5. In turbulent calculations, oxygen from the secondary inlet will typically diffuse in toward the centerline to react with the coal volatiles and with the residual char, but in this case, the diffusion rate is apparently so slow that the diffusing oxygen immediately reacts with the volatiles and none is available for reacting with the char. As a result, the char does not burn, and no further burnout occurs after devolatilization is complete, as shown in Figure III.A-6. This predicted behavior does not agree with observation. It seems that either the molecular diffusion rate is being incorrectly predicted, or the transport of oxygen is greater than the rate predicted by molecular diffusion alone, as evidenced by the fact that the particles have been observed to burn completely out. These predictions were made with a constant value for gas Schmidt number equal to 0.7, the value commonly used in turbulent flows. The effects of increasing the Schmidt number, and/or letting it vary locally are currently being investigated. Probably even more important than the effect of Schmidt number is the effect of locally generated turbulence by devolatilization, by combustion of the volatiles, by buoyancy effects, and by the aerodynamics of the particles. Buoyancy effects (free convection) could be taken into account by adding gravity terms to the gas equations of motion. The other effects cannot be predicted accurately by current methods, but may be predicted to a satisfactory degree by the k-epsilon turbulence model currently implemented in PCGC-2, but turned off for these calculations.

Converged solutions in laminar flow with the FG/DVC submodel have been difficult to achieve, apparently due to variation in the FG/DVC submodel predictions, and considerable effort has been expended in trying to pinpoint the source of the problem and correct it. For turbulent reactors, PCGC-2 typically converges from scratch in fewer than 15 particle iterations. The two convergence criteria in PCGC-2 are plotted as a function of particle iteration number for the Montana Rosebud case in Figure III.A-7. These criteria measure the change in the influence of the particles on the gas phase. One criterion is

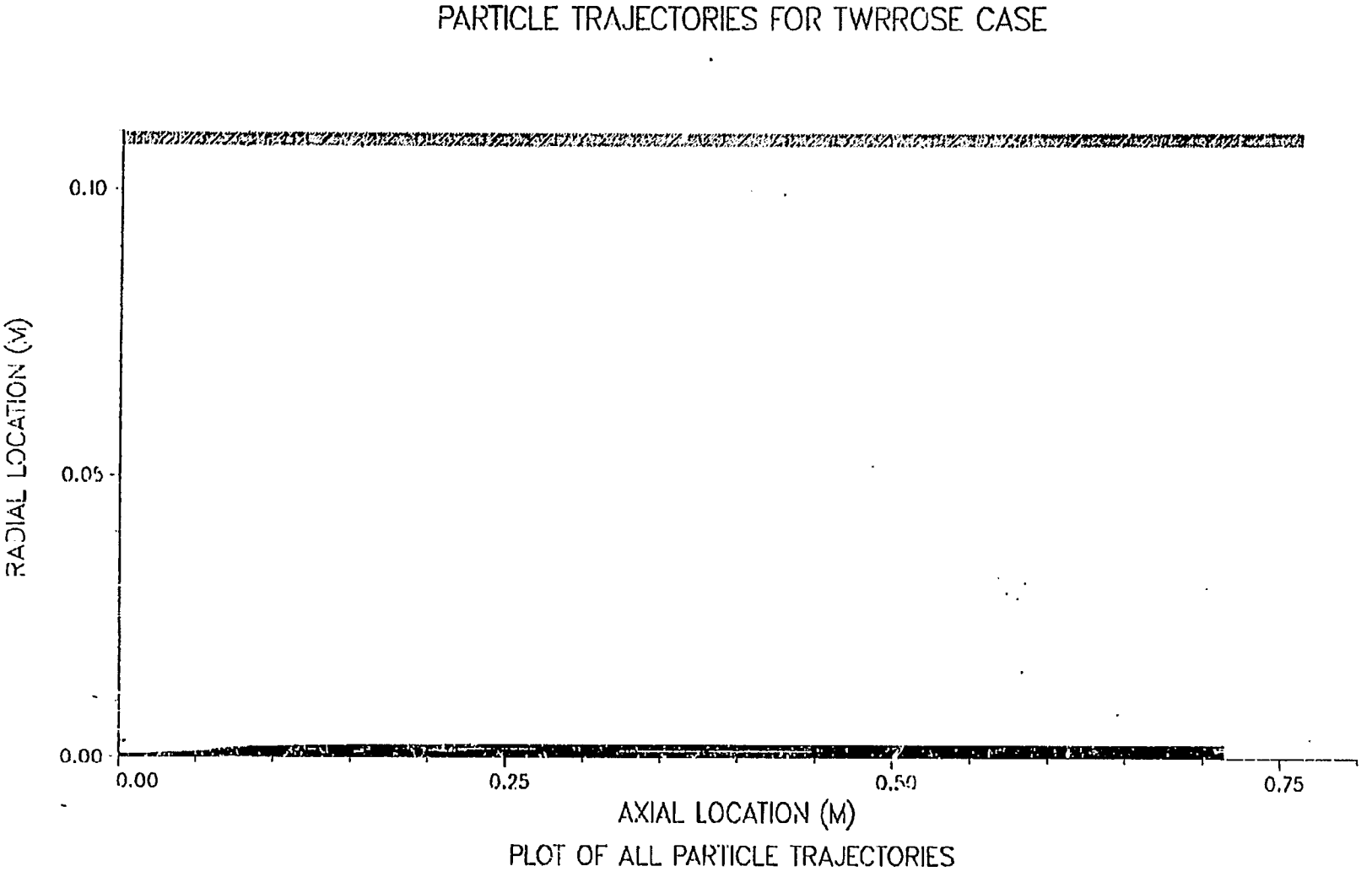


Figure III.A-3. Predicted particle trajectories for the combustion of Montana Rosebud coal in the transparent wall reactor.

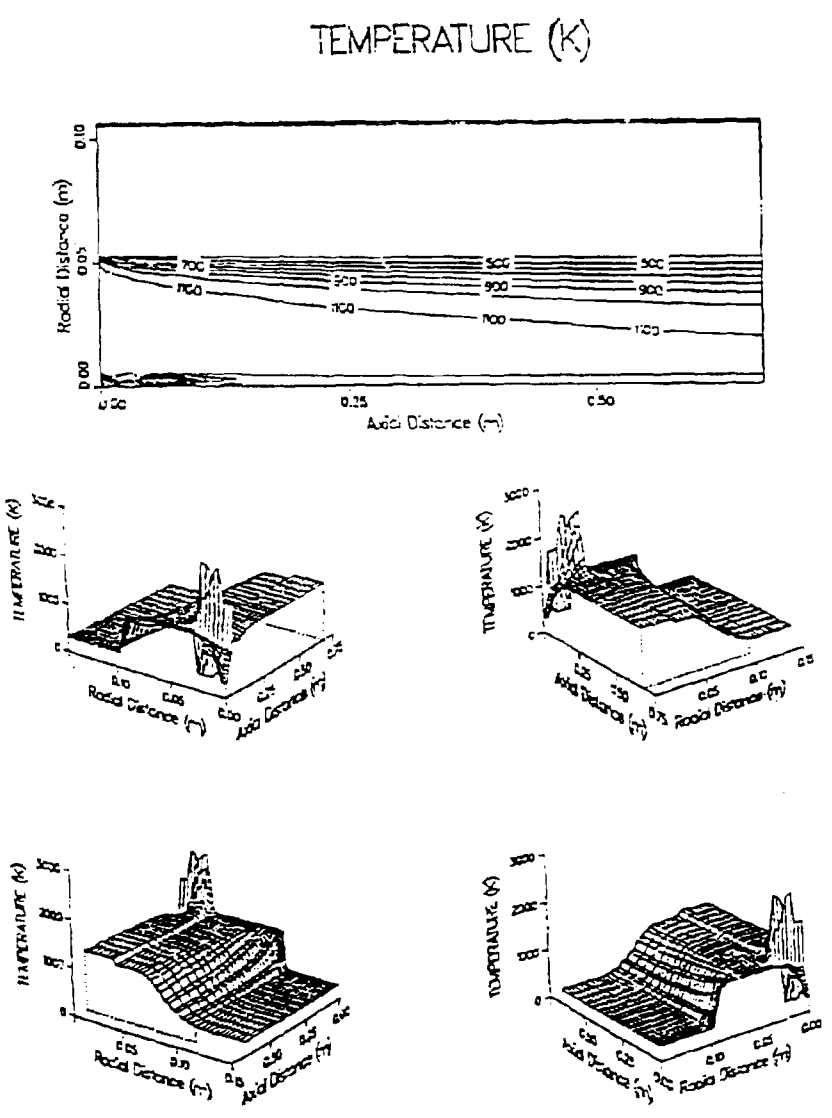


Figure III.A-4. Contour and surface plots of predicted gas temperature for the combustion of Montana Rosebud coal in the transparent wall reactor.

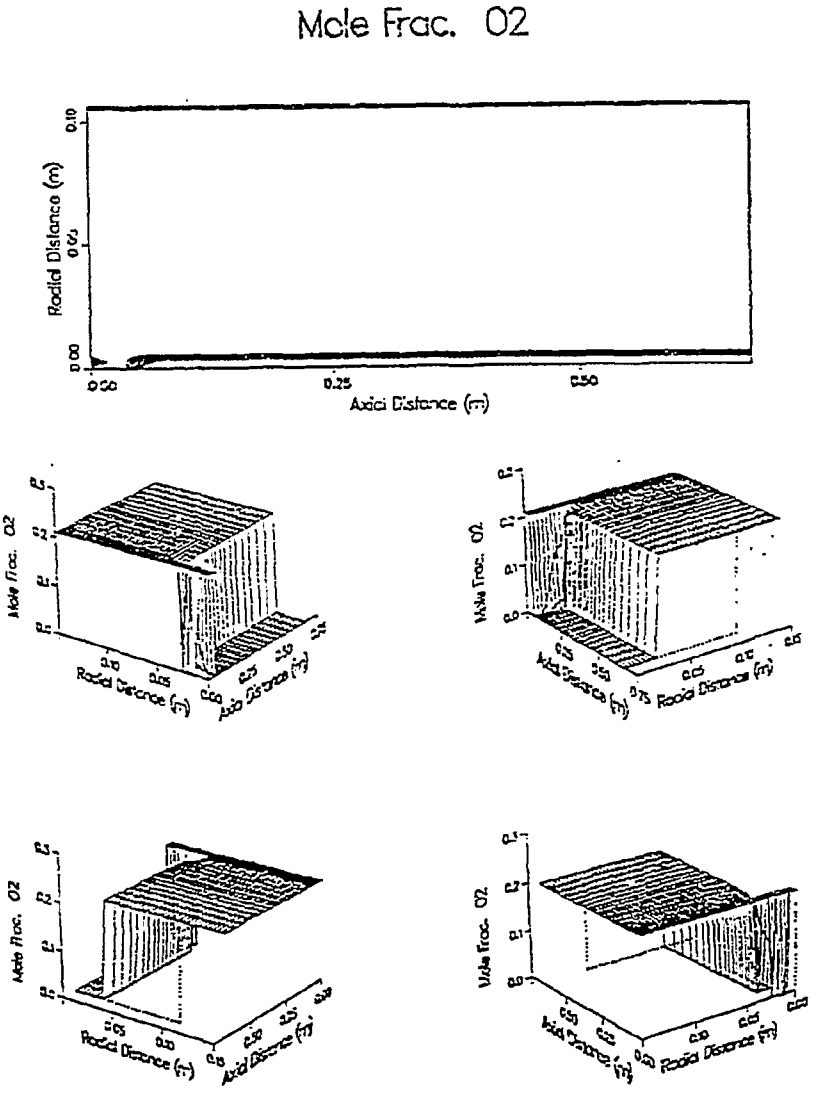


Figure III.A-5. Contour and surface plots of predicted gas oxygen concentration for the combustion of Montana Rosebud coal in the transparent wall reactor.

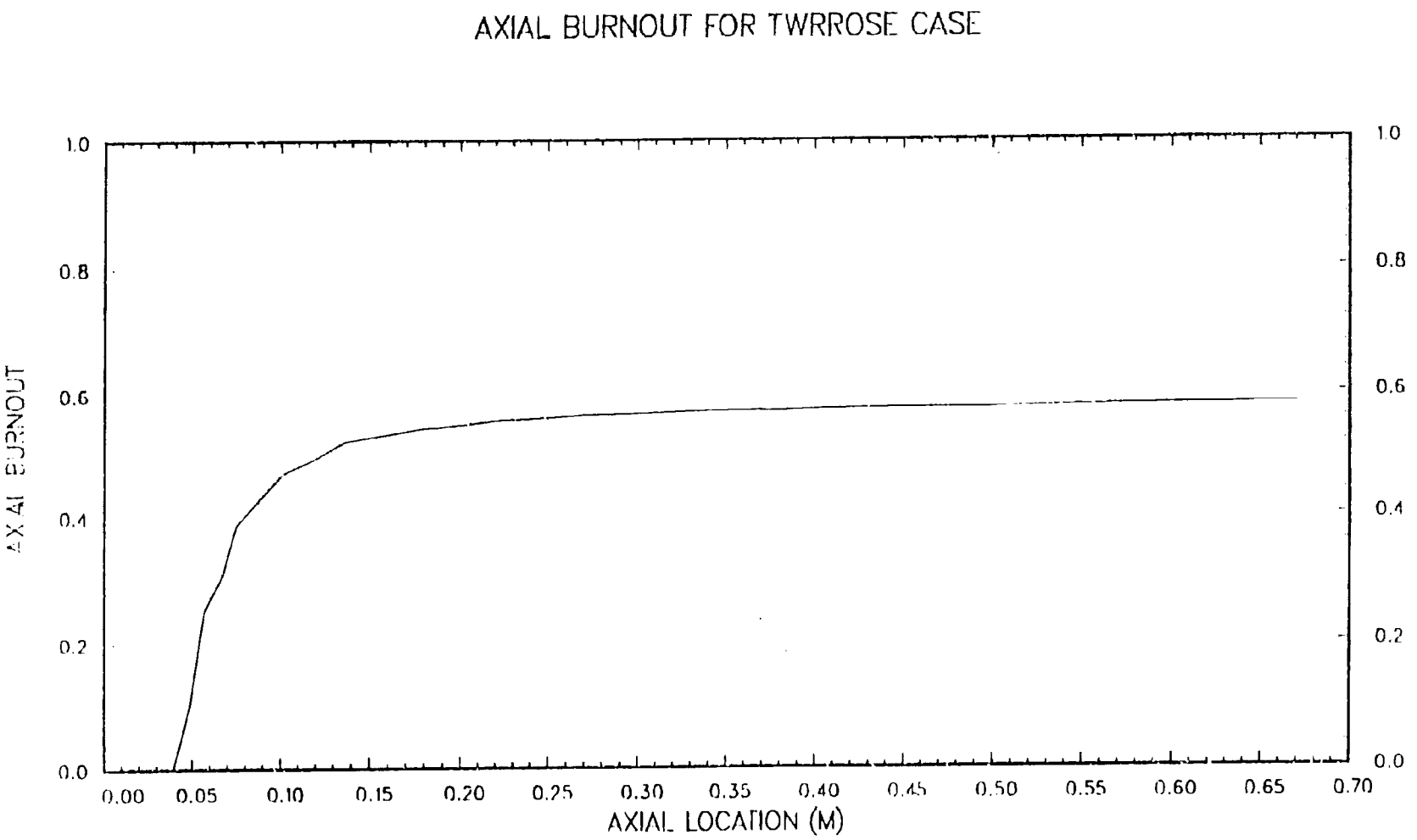


Figure III.A-6. Predicted particle burnout for the combustion of Montana Rosebud coal in the transparent wall reactor.

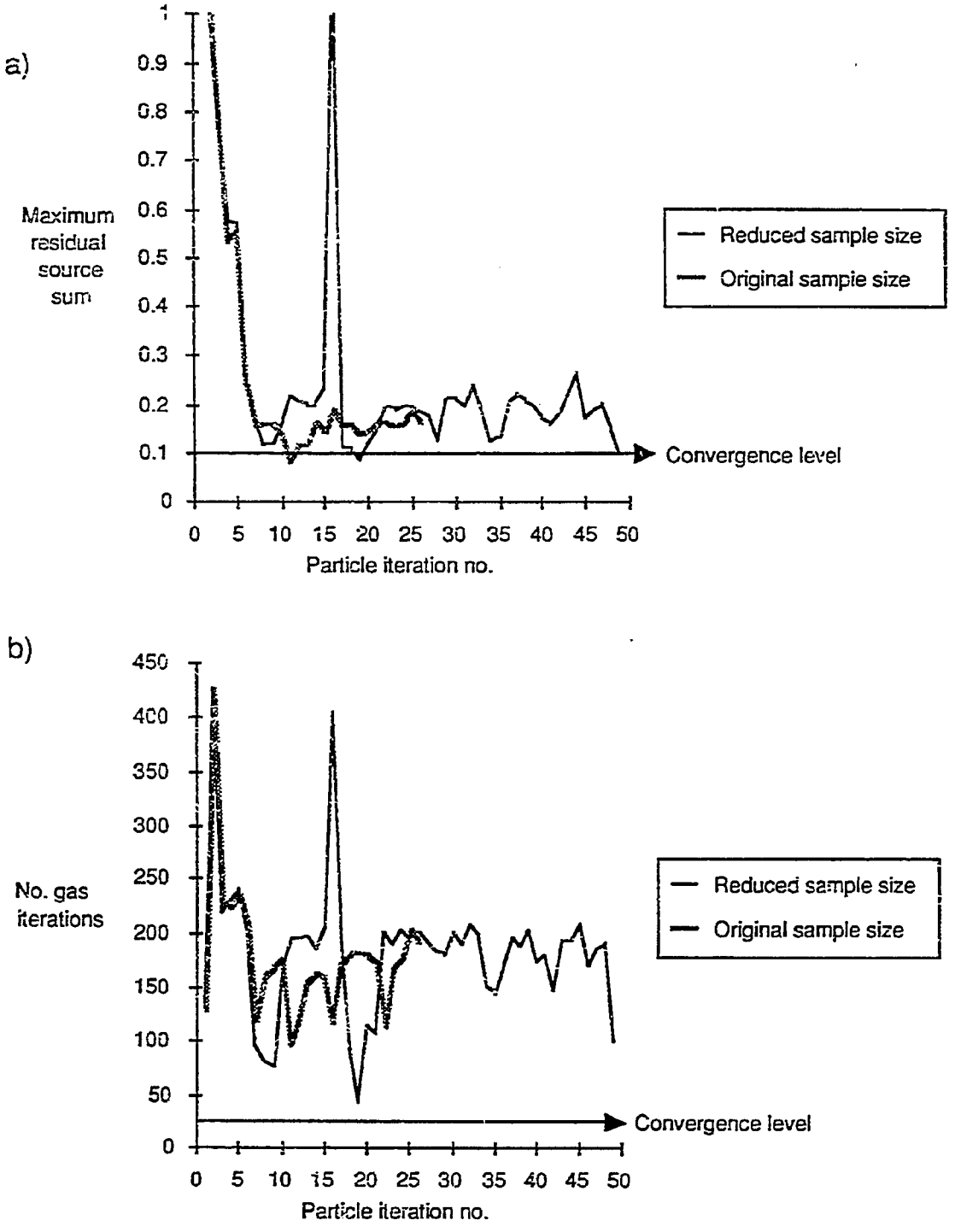


Figure III.A-7. Effect of coal polymer sample size on convergence of transparent wall reactor simulation for Montana Rosebud coal.

the maximum of the normalized residual source sums for all computational cells after a particle iteration. If the maximum residual source sum (converged to less than 0.01 prior to a particle iteration) increases by no more than a factor of 10 after a particle iteration, then overall convergence is typically assumed. The other criterion for overall convergence is the number of iterations required to reconverge the gas phase after a particle iteration. If the number of required gas iterations is less than a specified number (typically 25), overall convergence is assumed. As shown in the figure, both convergence criteria fluctuate randomly and fail to stabilize below their respective convergence levels. Predicted burnout also fluctuates unacceptably, as shown in Figure III.A-8. The exact reason for this behavior is not yet known and is being investigated. It has something to do with the random nature of the Monte Carlo method in the DVC portion of the submodel because, if a simple, two-step devolatilization model is substituted for the FG/DVC submodel, the problem goes away. Also, the laminar simulation converges normally if the FG/DVC submodel is used with the DVC portion of the submodel turned off.

Several possible reasons for the erratic convergence behavior are being investigated. One is that the coal polymer sample size (reduced to improve calculational efficiency) is too small. The DVC model input parameters that specify the sample size are shown in Table III.A-5. Values for both the original and reduced sample sizes are shown. When the original sample size was used, the fluctuations decreased somewhat in magnitude as shown in Figures III.A-6, 7 and 8, but they still continued at an unacceptable level, and there was no improved trend toward convergence. Additional calculations for particles in a uniform gas field showed that the problem is not due to an interaction of the Lagrangian particle calculations with the Eulerian grid spacing. Also, calculations for a single particle trajectory compared with those for 50 trajectories showed that the variation in the FG/DVC submodel predictions is lessened by averaging over multiple trajectories, as expected, however requiring more than 50 trajectories in order to smooth the FG/DVC submodel predictions is probably unacceptable. Other potential solutions to the problem are therefore being investigated, such as calling the FG/DVC submodel more frequently. Currently, the submodel is called when the particle temperature changes by at least 10 degrees.

TABLE III.A-5

PARAMETER VALUES USED IN THE INVESTIGATION OF THE EFFECT OF COAL SAMPLE SIZE ON FG/DVC SUBMODEL PREDICTIONS

| Coal Sample Size Parameters | Full Sample Size | Quarter Sample Size |
|---|---|---|
| Initial no. of oligomers (OLIGST) | 240 | 60 |
| Initial no. of hard bonds (FETHYL) | 900 | 225 |
| Initial no. of crosslinks (FLINK) | 290 | 72 |
| Initial no. of monomers (BEAD) | 2400 | 600 |

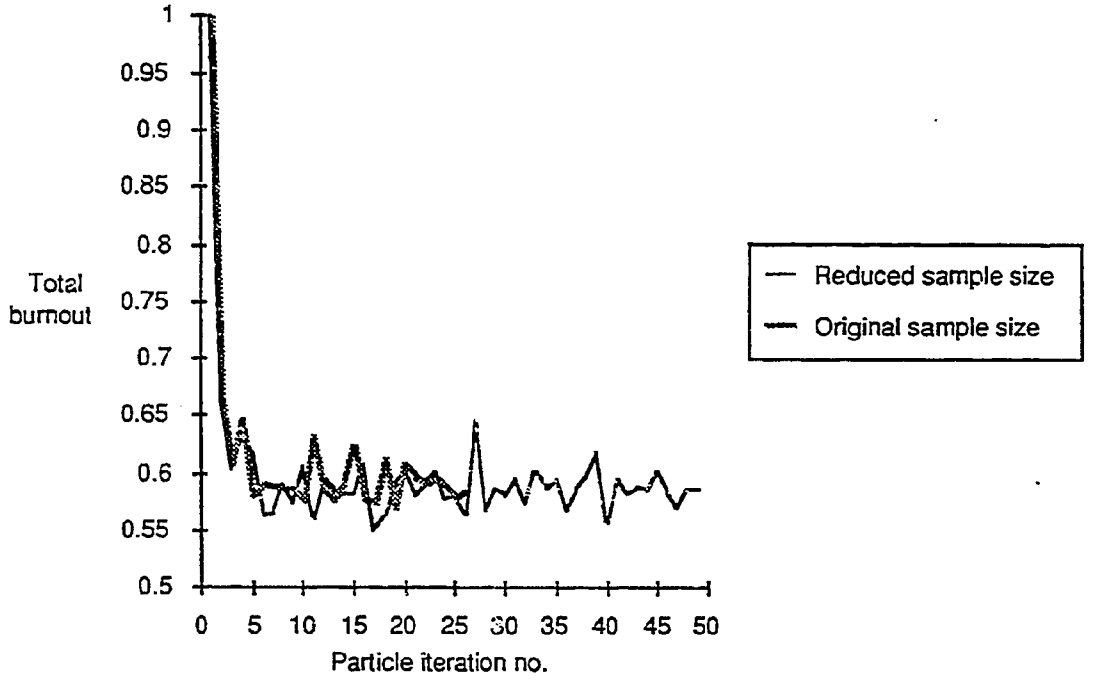


Figure III.A-8. Effect of coal polymer sample size on predicted total burnout for the combustion of Montana Rosebud coal in the transparent wall reactor.

Component 2 - Incorporating Improved Numerical Solution Methods

The purpose of this component of the subtask is to incorporate applicable improved numerical solution techniques that are being developed under separate funding. Work continued, under separate funding in this laboratory, during the past year to develop a multigrid method and incorporate it into a 3-D fluid mechanics code. This work is described under Project 5B in the Third Annual Report of the Advanced Combustion Engineering Research Center (Smoot et al., 1988). The multigrid method has already been demonstrated to significantly reduce computation time and increase the level of convergence that can be obtained in a 2-D fluid mechanics code (Christensen, 1988). The method uses multiple grids with varying resolution. Most of the computational work is performed on the coarser grids, requiring only periodic visits to the finer grids. At an appropriate time, the multigrid approach will be considered for incorporation into the 2-D code being developed in this study.

Component 3 - Incorporating $SO_x$-$NO_x$ Submodel

The aim of this subtask component is to incorporate the $SO_x$-$NO_x$ submodel being developed under Subtask 2.g into the comprehensive code, and to extend the comprehensive code to include sorbent injection and sorbent chemistry. Work continued during the past year on extending the pollutant submodel in PCGC-2 to include thermal NO. Work also continued under separate funding at The University of Utah (Pershing and coworkers) on the development of a sorbent reaction submodel with sulfur species and its incorporation into PCGC-2. The sorbent reactions submodel being developed in this study will be based on their work. Subtask 2.g provides further details on these two submodels.

Component 4 - Implementing the Code on Computers

The aim of this component of the subtask is to implement the comprehensive code on several computers, including workstations, and to assist AFR in implementing the code on their workstations. This implementation requires, at a minimum, standardizing the source code. A user-friendly graphics interface is also desirable. During the past year, the code has been implemented on Convex C-120 minisuper and C-210 supercomputers, and on Sun 3/210, 4/210, and 386i workstations, and a benchmark was run on each computer. The benchmark was the first sample problem given in the Revised PCGC-2 User's Manual (Smoot et al., 1988). The results are shown in Table III.A-6. A version of the code was also implemented at AFR on their Sun 3/210 workstation. In addition, graphics drivers have been developed and/or modified for the DISSPLA and UNIRAS graphics packages. Both of these packages are widely used in industry and run on a variety of computers and graphics devices, including Sun workstations. UNIRAS provides color capability, whereas DISSPLA does not. However, UNIRAS is limited in that it cannot create surface plots for non-uniform grid spacing. Work also continued during the year, under separate funding, on the development of a sophisticated color graphics package for 3-D applications that will also be applicable to 2-D (ACERC Third Annual Report, Smoot et al., 1988). Several color graphics plots prepared with UNIRAS and the new package being developed at BYU were shown in the 7th Quarterly Report (Solomon et al., 1988).

Table III.A-6

PCGC-2 BENCHMARKS

| Machine | Type | Cpu time |
|---|---|---|
| Sun 386i | Workstation | 10.8 hr |
| Sun-3/260 | Workstation | 7.0 hr |
| Sun-4/260 | Workstation | 3.5 hr |
| Convex C-120 | Minisuper computer | 2.5 hr |
| Convex C-210 | Super computer | 1.0 hr |

Component 5 - Code Evaluation

The goal of this subtask component is to evaluate the improved comprehensive code with advanced submodels and numerical methods incorporated under other components of the subtask. Two methods will be used. The first method for this evaluation uses a technique based on statistical experimental design theory as well as a global, non-linear sensitivity analysis. For the second method, various runs will be made and compared with experimental data. Detailed profile data and data that systematically vary one key parameter, such as coal type, stoichiometric ratio, etc., will be emphasized. Each is discussed below.

Sensitivity Analysis - An extensive parametric sensitivity study of PCGC-2 has been reported utilizing the simple, two-step devolatilization submodel (Smith and Smith, 1988). Their results illustrate the dominant effects that uncertainty in coal devolatilization/oxidation parameters have on uncertainty in predicted burnout, $NO_x$ formation, local gas temperature, and coal gas mixture fraction. They presented a series of plots illustrating the uncertainty in predicted mixing cup burnout, NO concentration, local gas temperature, and gas mixture fraction, with the fractional contributions (single partial variances) for the most significant input parameters. Devolatilization and oxidation parameters were among the most sensitive, with the uncertainty in activation energy for the high temperature devolatilization reaction accounting for over 80 percent of the uncertainty in predicted burnout and approximately 50 percent of the uncertainty in NO concentration. The burnout predictions were compared with experimental data, which, with the exception of two points, lay within the calculated uncertainty for the predicted burnout. The first data point outside the uncertainty range may be caused by inaccurate prediction of the ignition point. This disparity results from either the inability of the simple devolatilization submodel to predict ignition or inability to measure data accurately near the ignition point in a turbulent flame.

A similar analysis will be obtained with the integrated FG/DVC devolatilization submodel used in lieu of the two-step model. In this analysis, effects of the FG/DVC submodel parameters will be emphasized, since a complete sensitivity analysis for PCGC-2 would take as many as 350 runs per case

(see Smith and Smith, 1988). The sensitivity analysis performed by Smith and Smith (1988) included many parameters which did not influence the overall outcome as much as the devolatilization parameters. To reduce the required cpu time for the sensitivity analysis, a reduced set of parameters will be used in this study. To focus on major parameters in the FG/DVC submodel, a preliminary sensitivity analysis will be performed on a stand-alone version of the submodel model to determine which parameters seem to have significant effects on model predictions within their respective ranges of uncertainty. These parameters will then be used in the statistical sensitivity analysis, where other parameters are varied simultaneously and coupled effects are considered.

Comparisons with Data - To evaluate the impact of integrating the FG/DVC submodel into PCGC-2, detailed experimental data for comparison must be identified and collected. The following data categories have been identified: (1) laminar diffusion flames, (2) turbulent diffusion flames without swirl, and (3) turbulent diffusion flames with swirl. All three categories may include both combustion and gasification cases. Turbulent flow cases will be taken, in part, from an existing databook (Christensen et al., 1987). This collection consists of 35 sets of data from 8 laboratories. These cases were selected from 198 cases based on criteria which include data completeness, detailed digital profiles for several properties (e.g., species concentrations, velocity, temperature), and data accuracy. Only 15 of the 35 sets of data were either coal combustion or gasification results. The remaining sets were either non-reacting flows or gaseous combustion cases. (There was one coal slurry combustion case reported.) At least two turbulent flow cases will be selected from the databook.

Laminar cases will be obtained from the literature and from AFR measurements. Laminar flames eliminate the uncertainty associated with random turbulent fluctuations. For example, ignition points measured in laminar flames are expected to be more reliable than those measured in turbulent flames. Comparisons with laminar flame data may illustrate the need for the generalized devolatilization submodel in comprehensive combustion models by showing a definite improvement in prediction of such phenomena as ignition point.

A useful technique for model evaluation is to run cases where one major variable is systematically changed. Variables of interest may be coal type, stoichiometric ratio, swirl, nozzle type, etc. Trend analysis of predicted results such as burnout, ignition point, or $NO_x$ concentration can then be performed by comparing results from PCGC-2 with the integrated FG/DVC model and the simple two-step model.

## Plans

During the next quarter, work will continue on (1) evaluating and improving the operation of the FG/DVC submodel option in PCGC-2, (2) monitoring ongoing work under independent funding in this laboratory to develop and implement the multigrid method in a 3-D combustion code, (3) extending the pollutant submodel in PCGC-2 to include thermal NO and sulfur species and assisting The University of Utah with the integration into PCGC-2 of their sorbent capture submodel, (4) running the code on a variety of computers and workstations and implementing graphics, and (5) simulating the AFR transparent wall reactor with PCGC-2 to aid in validating the FG/DVC submodel. Work will be initiated on implementing the energy equation option in PCGC-2 with the FG/DVC submodel, and consideration

will be given to utilizing an improved numerical scheme for solving the particle equations and/or implementing a new energy equation solution method for the gas phase.

# III.B. SUBTASK 3.B. - COMPREHENSIVE FIXED-BED MODELING REVIEW, DEVELOPMENT, EVALUATION, AND IMPLEMENTATION

Senior Investigators - Predrag T. Radulovic, Sung-Chul Yi*,
L. Douglas Smoot, and B. Scott Brewster
Brigham Young University
Provo, Utah 84602
(801) 378-3097, (801) 378-4326, (801) 378-6240

*Philip Morris USA,
Richmond, VA 23261
(804) 274-2001

## Objectives

The objectives of this subtask are: 1) to provide a framework for an advanced fixed-bed model suitable for incorporating the advanced submodels being developed under Task 2, particularly the large particle submodel (Subtask 2.e), and 2) to provide a basis for evaluating the advanced model. Development of the basic framework of the model and initial integration of the large particle submodel will take place during Phase I.

## Accomplishments

Phase I of this subtask has three components: 1) a literature review and evaluation of existing fixed-bed coal gasification models and experimental data, 2) a detailed plan for an advanced fixed-bed model, and 3) development of the framework for an advanced fixed-bed model. Accomplishments under each subtask component are described below.

### Component 1 - Literature Review and Evaluation

This subtask component was aimed at 1) reviewing existing models for fixed-bed coal gasification to determine elements that might be useful for developing the advanced model, and 2) locating experimental data that can be used for model validation.

Review of Existing Models - A detailed review of existing models was described in the first annual report. Based on the review, a recommendation was made that an advanced model be developed.

Evaluation of existing models continued during the second year. Predictions obtained from the Washington University 2-D model were compared with experimental values, and a sensitivity analysis was performed. The model was run with Illinois bituminous coal (low reactivity) and Wyoming subbituminous coal (high reactivity). The ultimate and proximate analyses of these coals were obtained from Cho (1980). Oxygen-blown, dry-ash operation of a Lurgi gasifier was modeled. Specific operating conditions for each case were obtained from Yoon, et al. (1978). Comparisons of the predicted product compositions with experimental data for the Washington University (WU) and University of Delaware (UD) 1-D and 2-D codes are given in Figures III.B-1 and III.B-2.

For the Illinois coal, the WU 1-D model predicted too much hydrogen, too little carbon dioxide, and too little methane in comparison with plant data (Yoon, et al., 1978). The results of the WU 2-D model gave some improvement. Overall product gas distribution predicted by the WU 2-D model was best among the four sets of model predictions.

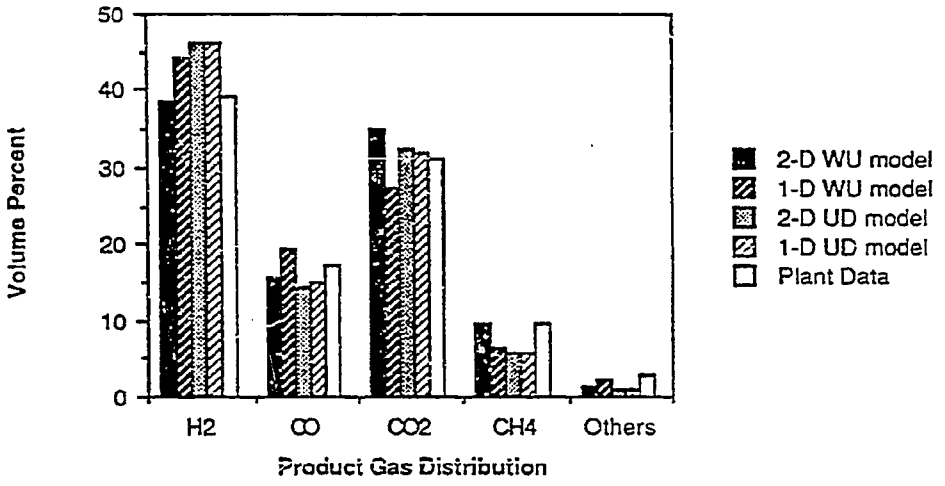


Figure III.B-1. Comparison of product composition predicted by various codes with plant data for Illinois coal.

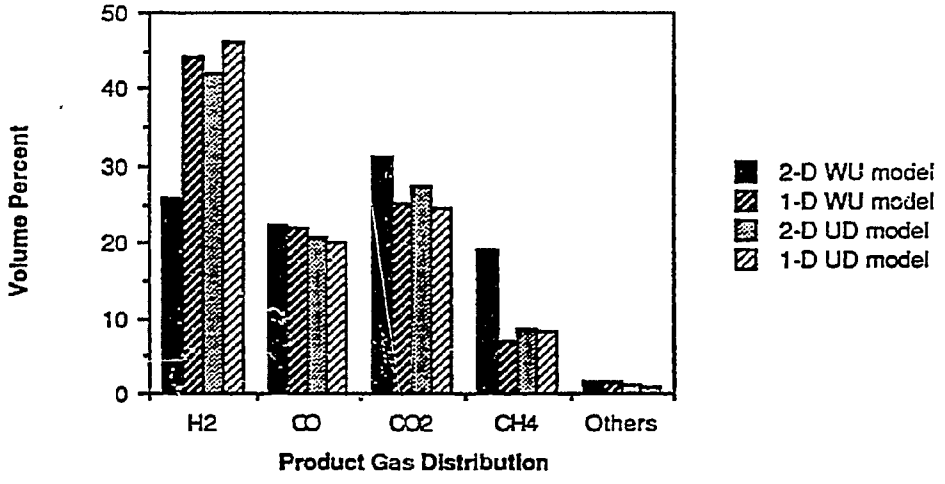


Figure III.B-2. Comparison of product composition predicted by various codes for Wyoming coal.

There are no experimental data available for the Wyoming coal case. Therefore, only model predictions are shown in Figure III.B-2. The WU 2-D model predicts less hydrogen and more methane than the other models. Also, the predicted carbon dioxide is higher than for the other three models. It should be emphasized that prediction of effluent gas composition is a very limited test of model validity or utility.

The sensitivity analysis was performed on gas inlet temperature, heat transfer coefficient, and wall temperature. As input to the WU 2-D model, the inlet gas temperature must be specified. The inlet temperature was varied from the base case of 644 K to 544 K and 744 K. The effect of gas inlet temperature on product gas composition is shown in Figure III.B-3. As inlet temperature increases, hydrogen and carbon monoxide increase while methane and carbon dioxide decrease. Methane and hydrogen changed by less than one percent over the 200 K temperature range. However, carbon dioxide and carbon monoxide changed significantly. The WU 2-D model assumes that the molar ratio of carbon monoxide/carbon dioxide in the combustion reaction follows an Arrhenius temperature relation (Rossberg, 1956). Thus, changes in $T_g$ significantly impact the $CO/CO_2$ ratio.

Increasing the wall temperature from the 496 K to 796 K had virtually no effect on the maximum temperature. Figure III.B-4 illustrates that increasing the wall temperature by 200 K did affect the outlet gas temperature, increasing it by 80 K.

The base case was run with a heat transfer coefficient of 340 $kJ/m^2$-hr-K. Decreasing the value of the coefficient to 140 $kJ/m^2$-hr-K reduced the amount of heat loss to the surroundings and increased the outlet temperature by 15 K. However, the outlet temperature decreased by 20 K when the heat transfer coefficient was raised to 540 $kJ/m^2$-hr-K, as shown in Figure III.B-5. Maximum temperature was fairly insensitive to variation in heat transfer coefficient.

Review of Flow, Mass, and Heat Transfer - Flow, mass, and heat transfer processes in fixed-bed gasifiers are very complex. Coarsely crushed coal settles while undergoing heating, drying, devolatilization, gasification, and combustion. Polydisperse coal particles change diameter, shape, and porosity. The coal bed permeability changes, too. There may be coal bridges, gas bubbles, and channels. Gases flowing upward are heated and take part in a number of chemical reactions. Variations in bed permeability and possible formation of bubbles and channels also affect flow and pressure drop. Mass transfer occurs by diffusion and convection. Heat transfer is by conduction, convection, and radiation in the gas and solid phases.

A summary of correlations being considered for an advanced fixed-bed model is presented in Table III.B-1. Plug flow has been commonly assumed for the solid phase. However, consideration should be given to the structural properties affecting the settling of coarse, crushed coal (Hauserman, 1984), and to the channeling effect in beds with variable permeability (Vafai, 1986). The friction factor for the gas phase can be calculated by Ergun's equation (1952). MacDonald, et al. (1979) have recently compared the Ergun equation with a large number of experimental data, and concluded that the Ergun equation is superior to others proposed in the literature for the wide porosity ranging from 0.36 to 0.92, whereas other equations are better for narrower porosity ranges. The

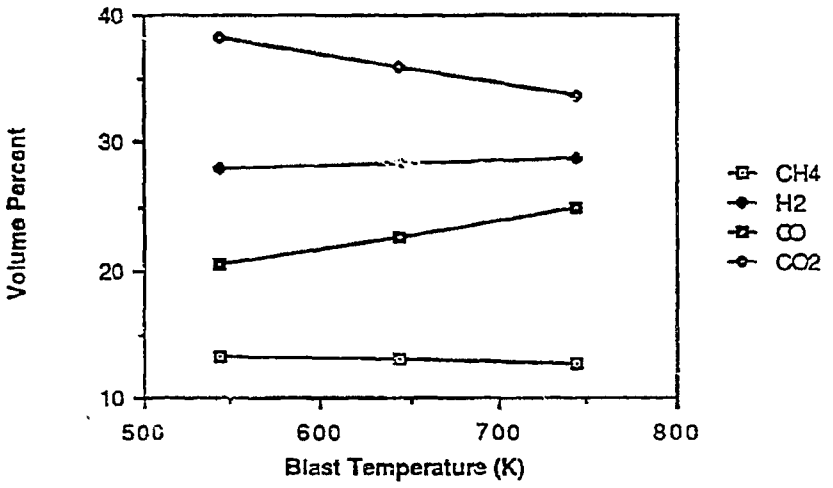


Figure III.B-3. Effect of gas inlet temperature on product gas composition.

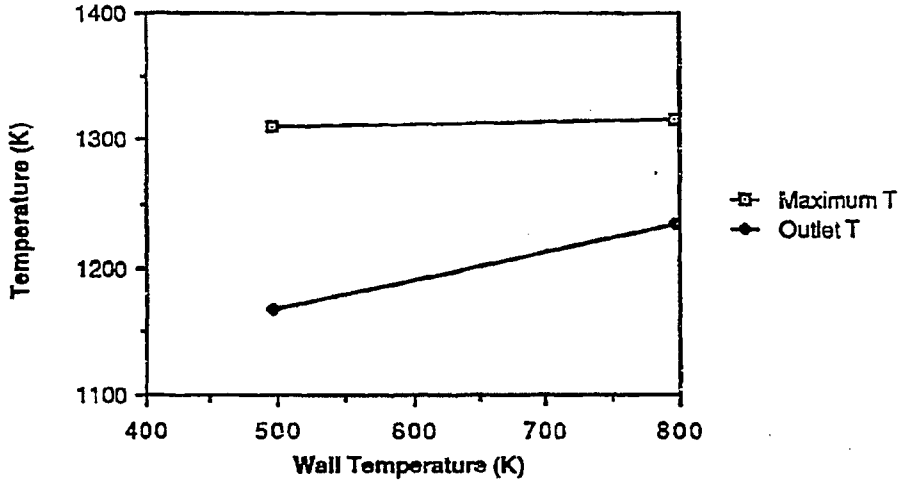


Figure III.B-4. Effect of wall temperature on gasifier temperature.

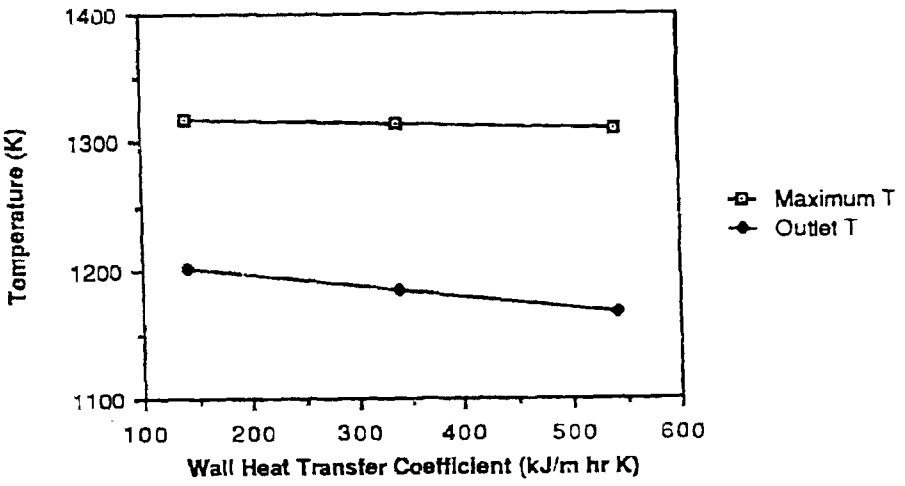


Figure III.B-5. Effect of heat transfer coefficient on gasifier temperature.

Table III.B-1. Flow, Mass and Heat Transfer Coefficients in Moving-Bed Reactor

| Eq. No. | Coefficients | Correlations | References |
|---|---|---|---|
| (III.B-1) | Friction factor for gas phase | $f = \frac{1-\phi}{\phi^3}(1.75 + 150\,\frac{1-\phi}{Re})$ for $\frac{Re}{1-\phi} < 500$ | Ergun (1952) |
| (III.B-2) | Particle-to-fluid mass transfer coefficient | $k_{g,i} = \frac{1.66G}{M_m p f_{a,i}} Re^{-0.51} Sc^{-2/3}$ for $Re < 190$, $\phi = 0.37$ spheres<br>$k_{g,i} = \frac{0.983G}{M_m p f_{a,i}} Re^{-0.91} Sc^{-2/3}$ for $Re > 190$, $\phi = 0.37$ spheres | Froment and Bischoff (1979) |
| (III.B-3) | Particle-to-fluid heat transfer coefficient | $h_p = \frac{2.06 f C_p G}{\phi} Re^{-0.575} Pr^{-2/3}$ | Gupta and Thodos (1963) |
| (III.B-4) | Effective axial diffusivity | $D_{ea} = \frac{U_{g,s} d_p}{1.5}$ | Froment and Bischoff (1979) |
| (III.B-5) | Effective radial diffusivity | $D_{er} = \frac{U_{g,r} d_p}{7\left[1 + 46 (d_p/D_f)^2\right]}$ | Froment and Bischoff (1979) |
| (III.B-6) | Effective axial conductivity | $K_a = K_{ea}^s + K_g \delta_1 PrRe$ for $Re < 50$<br>$K_a = K_{ea}^s + K_g \left(\delta_1 PrRe + \delta_2 Pr^2 Re^2 \frac{1}{\frac{K_{ea}^s}{K_g} + \delta_1 PrRe}\right)$ for $Re > 50$ | Yagi et al. (1960); Bischoff (1962) |

Table III.B-1. Flow, Mass and Heat Transfer Coefficients in Moving-Bed Reactor
(Continued)

| Eq. No. | Coefficients | Correlations | References |
|---|---|---|---|
| (III.B-7) | Effective radial conductivity | $K_r = K_g[\phi(1+\beta\frac{h_{rv}d_p}{K_g}) + \frac{(1-\phi)\beta}{\frac{1}{\frac{h_p d_p}{K_g} + \frac{1}{\chi} + \frac{h_{rs}d_p}{K_g}} + \gamma\frac{K_g}{K_s}}] + K_g\frac{PrRe}{Pe_r}$ | Froment and Bischoff (1979) |
| (III.B-8) | Effective radial gas conductivity | $K_{gr} = K_g[\phi(1+\beta\frac{h_{rv}d_p}{K_g}) + \frac{PrRe}{Pe_r}]$ | DeWasch and Froment (1971) |
| (III.B-9) | Effective radial solid conductivity | $K_{sr} = K_g[\frac{(1-\phi)\beta}{\frac{1}{\frac{h_p d_p}{K_g} + \frac{1}{\chi} + \frac{h_{rs}d_p}{K_g}} + \gamma\frac{K_g}{K_s}}]$ | DeWasch and Froment (1971) |
| (III.B-10) | Bed-To-wall effective heat transfer coefficient | $h_w = 2.44\frac{K^s_{er}}{D_t^{4/3}} + 0.033\frac{K_g PrRe}{d_p}$ | DeWasch and Froment (1971) |
| (III.B-11) | Bed-to-wall heat transfer coefficient for gas phase | $h^g_w = \frac{K_{gr}}{K_{gr} + K_{sr}}h_w$ | DeWasch and Froment (1971) |
| (III.B-12) | Bed-to-wall heat transfer coefficient for solid phase | $h^s_w = \frac{K_{sr}}{K_{gr} + K_{sr}}h_w$ | DeWasch and Froment (1971) |

problems of non-isothermal reacting flow with variable porosity and channeling remain to be investigated.

The particle-to-fluid mass transfer coefficient is correlated by Froment and Bischoff (1979). Alternatively, correlations are suggested by Gupta and Thodos (1963) and used by Denn, et al. (1982) and Bhattacharya, et al. (1986). The influences of porosity and asphericity remain to be determined. The particle-to-fluid heat transfer coefficient can be estimated by Gupta and Thodos' correlation (1963). Initially, the particles will be assumed to be uniform throughout. Later, intraparticle mass and heat transfer will be considered. Effective axial and radial diffusivities are correlated by Froment and Bischoff (1979), and by DeWasch and Froment (1971), respectively. Turbulent diffusion is assumed to be dominant in both directions.

Effective axial and radial conductivities are correlated by Yagi, et al. (1960) and Bischoff (1962), and by Froment and Bischoff (1979), respectively. Both the axial and radial effective conductivities take into account molecular as well as turbulent contributions. The effective radial conductivity accounts for radiation. It should be noted that both correlations lump the gas and the solid phases together. There is no available information on the effective axial conductivities of the gas and solid phases separately. The gas and solid phase contributions to the effective axial conductivity may be determined by analogy to the effective radial conductivity, if needed. Yagi, et al. (1960) noted that at low flow rates, axial conductivity cannot be neglected. The effective conductivity is also given by Rohsenow et al. (1985). The effective radial conductivities of the gas and solid phases are correlated by DeWasch and Froment (1971). The same modes of the heat transfer are taken into account as for the lumped conductivities. Later, a diffusion approximation for radiative heat transfer will be considered.

The effective bed-to-wall heat transfer coefficient as well as the gas and solid phase contributions are determined by the correlations suggested by DeWasch and Froment (1971). The heat transfer to the wall is treated by Yagi and Wakao (1959) and Yagi and Kunii (1960). Additional information is given by Rohsenow, et al. (1985). There are no direct experimental data available on the gas and solid phase contributions to the bed-to-wall heat transfer.

Review of Fixed-Bed Technology - This review is limited to fixed-bed gasification. Stoker boilers are not considered. Fixed-bed gasification is one of two leading technologies for 1) production of fuel gas from coal; 2) integrated gasification, combined-cycle electrical power generation (IGCC); 3) production of synthesis gas from coal; and 4) retrofitting oil-fired power plants, fuel cells, etc. Fixed-bed gasification is the most important commercial gasification process. Eighty-nine percent of the coal is gasified by fixed-bed (Lurgi), ten percent by entrained-bed (Koppers-Totzek), and only one percent by fluid-bed (Winkler). Lurgi's dry ash gasification process is the only commercial fixed-bed gasification process. Fixed-bed reactors may be conveniently divided into commercial, demonstration, development, and laboratory units, as shown in Table III.B-2.

Collection of Data - The collection of fixed-bed reactor design and test data was continued. Design and test data have been collected for some of these fixed-bed reactors, as summarized in Table III.B-2. Particular attention was paid to mild gasification data. UCC Research Corporation's mild gasification

**TABLE III.B-2**
**Fixed-Bed Reactors Test Data**

## Commercial

1. LURGI Dry ash

   - o Sasolburg and Secunda (SASOL), South Africa -- Not available

   - o Westfield, Scotland (1974)
     J. Stefano (1985) and Woodall-Duckham (1974)
     Effluent data, height of combustion zone, variations in coal type, some variations in operating parameters

   - o Beulah (Great Plains), North Dakota (1984)
     B.W. Benjamin (1985), I.H. Ringard and B.W. Benjamin (1985)
     Some design data, no experimental data

## Demonstration

1. BGC/LURGI Slagging Ash

   - o Westfield, Scotland (1981)
     J.E. Scott (1981) and J. Stefano (1985)
     Effluent data, Pittsburgh No. 8 coal, some variations in operating parameters, solid flow problems, dynamic behavior, gas dust loading, excellent

2. KILnGAS

   - o Wood River Station, Illinois -- Not available

## Development

1. METC -- Morgantown, West Virginia

   - o K. Pater (1986), J. Stefano (1985) and other METC publications
     Effluent and some other data, variations in coal type, variations in operating conditions, $O_2$ vs. air, sophisticated measurements (CARS, etc.), the 2nd most comprehensive set of data available

2. MGU -- Bristol, Virginia

   - o C.I.C. Chu and B.L. Gillespie (1987)
     Some design data, no experimental data

## TABLE III.B-2
## Fixed-Bed Reactors Test Data (Continued)

**Development** (Continued)

3. Wellman-Galusha -- Minneapolis, Minnesota

   - o D. Thimsen, et al. (1984, 1985), data book soon
     Effluent data, many U.S. coals, axial profile data on pressure and temperature, operational procedure, monitoring procedure, test procedure, calculation and data analysis procedure, all dimensions of gasifier, detailed data on measuring equipment, the most comprehensive set of data available

4. GEGAS -- Schenectady, New York

   - o K.J. Daniel and P.P. Shah (1980), J. Stefano (1985), Corman, et al. (1984)
     Effluent data only, some variations in operating parameters

5. GFETC -- Grand Forks, North Dakota

   - o J. Stefano (1985)
     Effluent data, height of combustion zone, some variations in operating conditions

6. RUHR 100 -- Dorsten, West Germany -- Not available

7. KGN -- Hueckelhoven, West Germany -- Not available

**Laboratory**

1. Washington University -- St. Louis, Missouri

   - o A. Bhattacharya, et al. (1986), A. Bhattacharya (1985), L. Salam (1983)
     Effluent data, axial temperature profile, unsteady data

2. Pennsylvania State University -- University Park, Pennsylvania

   - o A. Barriga and R.H. Essenhigh (1980), T. Eapen, et al. (1977), T. Eapen (1979)
     Effluent data, axial temperature and gas composition profiles

program will probably provide some of the needed test data. The Eighth Annual Gasification and Gas Steam Cleanup Systems Contractors Review Meeting at Morgantown, WV, was attended. A number of presentations and posters were devoted to fixed-bed gasification and in particular to mild gasification. The Morgantown Energy Technology Center (METC) was visited, including a tour of the METC fixed-bed reactor.

Comprehensive Review - A comprehensive review of fixed-bed combustion and gasification was initiated. The first draft is being prepared. The review will include a summary of experimental observations, large particle reaction rates, models for fixed-bed combustion and gasification processes, features of fixed-bed reaction processes and related technology. This review is an extension of the fixed-bed modeling review conducted under this project last year and is independently funded.

A section on large particle devolatilization was completed. A summary of mass and heat-transfer-limited devolatilization models is presented here. This discussion may also be pertinent to pulverized coal devolatilization depending on the heating rate experienced by the coal particles. Two types of devolatilization models emerge depending on the plasticity of the coal. A brief discussion on plasticity is also given to emphasize needed research in predicting plasticity.

**Plasticity** - The physical structure of the coal during pyrolysis is not completely understood. The individual particles may soften at devolatilization temperatures depending on rank, pressure, particle size, heating rate, etc. The physical transformation will also have a major impact on pore evolution. While no reliable means of differentiation exists, the plasticity, or swelling, correlates well with both volatile matter and carbon content for measurements made at 1 atm of inert gas and low heating rates, 0.01-0.20°C/s (Loison, et al., 1963). Swelling occurs for volatile contents of 15 to 40 percent and carbon contents of 81 to 92 percent with maxima near 30 and 89 percent, respectively. Lignites and anthracite fall outside these ranges, whereas low volatile bituminous coals generally exhibit the most marked plasticity (Russel et al., 1979). The heuristic values mentioned above are generally accepted; although, many factors such as pressure, particle temperature, heating rate, ambient gas composition, etc., may influence the fluidity of the coal. More work is needed to determine the conditions leading to fluid behavior.

The test conditions mentioned above do not correspond to conditions expected in a fixed-bed reactor, leaving uncertainties in what physical structure to assume. Several experiments indicate that softening becomes more pronounced at high pressure, high heating rate, and in hydrogen atmosphere (Loison et al., 1963). More work is needed to extrapolate softening characteristics to conditions of interest.

**Mass Transfer Limited Models** - Most of the models which account for mass transfer predict weight loss without product composition. The transport processes have been modeled by use of an empirical external mass transfer coefficient, pore transport within the particle, transport controlled by bubbles within the particle, liquid diffusion, film-diffusion similar to the classical droplet evaporation model, or combinations (Suuberg, 1985). Obviously, the wide spectrum of models imply different assumptions about the structure of the coal during devolatilization. Some approaches assume the particles to be porous

throughout pyrolysis, while others assume the particles to soften. None of these models apply universally to all coals.

Figure III.B-6 summarizes recent devolatilization models that incorporate transport models. A general outline of the two types of models is shown. Most models can be made to fit these two reaction schemes, depending on the assumption of softening coals versus non-softening coals. The reaction steps are numbered to distinguish between the various models.

Most devolatilization submodels used in fixed-bed models have been either mathematical curve-fit models or chemical models. No comprehensive fixed-bed model (reviewed in this study) has used a devolatilization submodel that includes mass or heat transfer limitations. Proper accounting for mass and heat transfer is important, since particle size effects can be included with a coupled heat and/or mass transfer submodel. Also, combined chemical/physical devolatilization models that apply to all coals (i.e., softening and non-softening coals) have not been found in the open literature.

Component 2 - Detailed Plan for Fixed-Bed Model

The purpose of this component of the subtask is to develop a detailed plan for an advanced fixed-bed model. From the review of existing models, it was concluded that the model should not be based on an existing model, but that a new model should be developed using appropriate elements of existing models. A research plan for developing the advanced code was formulated under Subtask 1.b and presented to METC and AFR at the First Annual Contract Review Meeting, which was held in Hartford, Connecticut, in November 1987.

A detailed explanation of the advanced model features and a development schedule are contained in the research plan which was submitted to METC. Generalizing coal reaction processes, extending the gas phase to consider more species, treatment of pollutants and radiation, and improved treatment of solids and gaseous flow processes are the principal areas of focus. The rationale for developing an advanced model includes the following:

- The past level of effort in fixed-bed modeling has been quite modest.
- There is currently no other known ongoing investigation in fixed-bed modeling.
- There is currently no generalized, robust, well-documented code for fixed-bed coal gasification available.
- There has been little evaluation and application of fixed-bed models.
- Fixed-bed technology is of considerable current interest in high-pressure combined-cycle power generation, synthesis gas production, liquids production (mild gasification), fuel gas production, and combustion.
- The importance of fixed-bed technology was specifically noted in two COGARN (Penner, 1987) recommendations.

Figure III.B-6. Generalized Scheme for Devolatilization Models with Mass Transfer Submodels

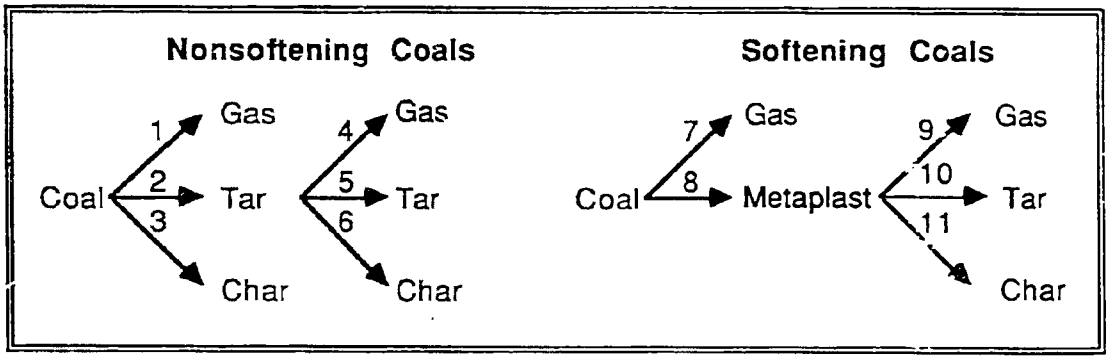


| Model | Sequence |
|---|---|
| 1. Anthony *et al.* (1974) | 1-4, 6 |
| 2. Mill *et al.* (1976) | 1, 3 (repeated in three sequential steps) |
| 3. Lewellen (1975) | 1, 2 (into bubbles), 3, 5, 6 |
| 4. Melia and Bowman (1983) | 1&2 going to 4&5, 3 |
| 5. Russel (1979) | 1-3, 5, 6 |
| 6. Chen and Wen (1975) | 2-6 |
| 7. Devanathan and Saxena (1985, 1987) | 1-4,6 |
| 8. Solomon *et al.* (1988) | 1-5 |
| 9. Suuberg *et al.* (1979) | 7, 8, 10, 11 |
| 10. Unger and Süuberg (1981) | 7, 8, 10, 11 |
| 11. Schaub *et al.* (1985) | 7-11 |
| 12. Bliek *et al.* (1985) | 7-9, 11 |

- The COGARN report (1987, p. 35) specifically recommends development of fixed-bed process models.

- Large particle tests being conducted under Subtasks 2.e and 2.f provide significant support to the development of the model.

- Developing the entrained-bed code and the advanced fixed-bed model simultaneously would be complimentary and synergistic.

Component 3 - Development of the Framework for an Advanced Fixed-Bed Model

The purpose of this component of the subtask is to develop a code framework for an advanced fixed-bed model. The physical and chemical processes in a typical fixed-bed coal gasifier are illustrated in Figure III.B-7. Coal is fed through a lock hopper to a distributor at the top of the bed. Gas (e.g., oxygen and steam) is fed to the bottom of the reactor. The coal moves slowly downward through the bed where it is progressively dried and devolatilized, the residual carbon is gasified and combusted, and the ash is removed through a grate into another lock hopper. The product gas is removed from the top of the gasifier and quenched. The bed zones shown in Figure III.B-7 are for illustrative purposes only. The curvature in the zone boundaries is meant to illustrate the effect of radial temperature gradients in the bed. Obviously, such distinct zones do not exist in reality, since the drying, devolatilizing, gasifying, and combusting processes are one continuous operation. Also, because of intraparticle temperature gradients and variance in particle size and shape, the particles do not react uniformly. However, it is useful to keep this idealized picture in mind when discussing the formulation of the proposed model.

Improved Fixed-Bed Model - As a basis for the advanced fixed-bed model, work was initiated on an improved model. The improved fixed-bed model has many of the basic features of an advanced model, such as separate gas and solids temperatures, but is simplified in its treatment of chemistry and numerical solution method. The improved model was designed to test many of the important features of the advanced model.

The improved fixed-bed model has been formulated and coded (Yi et al., 1988). The improved model is a two-dimensional, axisymmetric, counterflow model. It is similar to the Washington University model (Bhattacharya et al., 1986), but is extended to include separate gas and solids temperatures, accumulation of energy and mass in the gas phase, radial dispersion of mass in the gas phase, and motion of the solid phase. The dynamics of the gasifier are dominated by accumulation of mass and energy in the solid phase. Still, the accumulation terms in the gas phase are included because of the mathematical simplicity of the resulting equations. The radial thermal conductivities of gas and solid, the wall heat transfer coefficient, and the gasifier wall temperature are all assumed constant. Axial mixing of mass and energy is neglected based on the criterion of Young and Finlayson (1973). Both solid and gas phases are assumed in plug flow. Solid velocity and bed porosity are assumed constant.

Both drying and devolatilization have been assumed to occur instantaneously by previous investigators, since the time required for these two events is of the order of a few seconds compared to a total residence time of hours for the coal. In the advanced model, a detailed devolatilization submodel will be incorporated. Therefore, a segregated, but finite, devolatilization process is

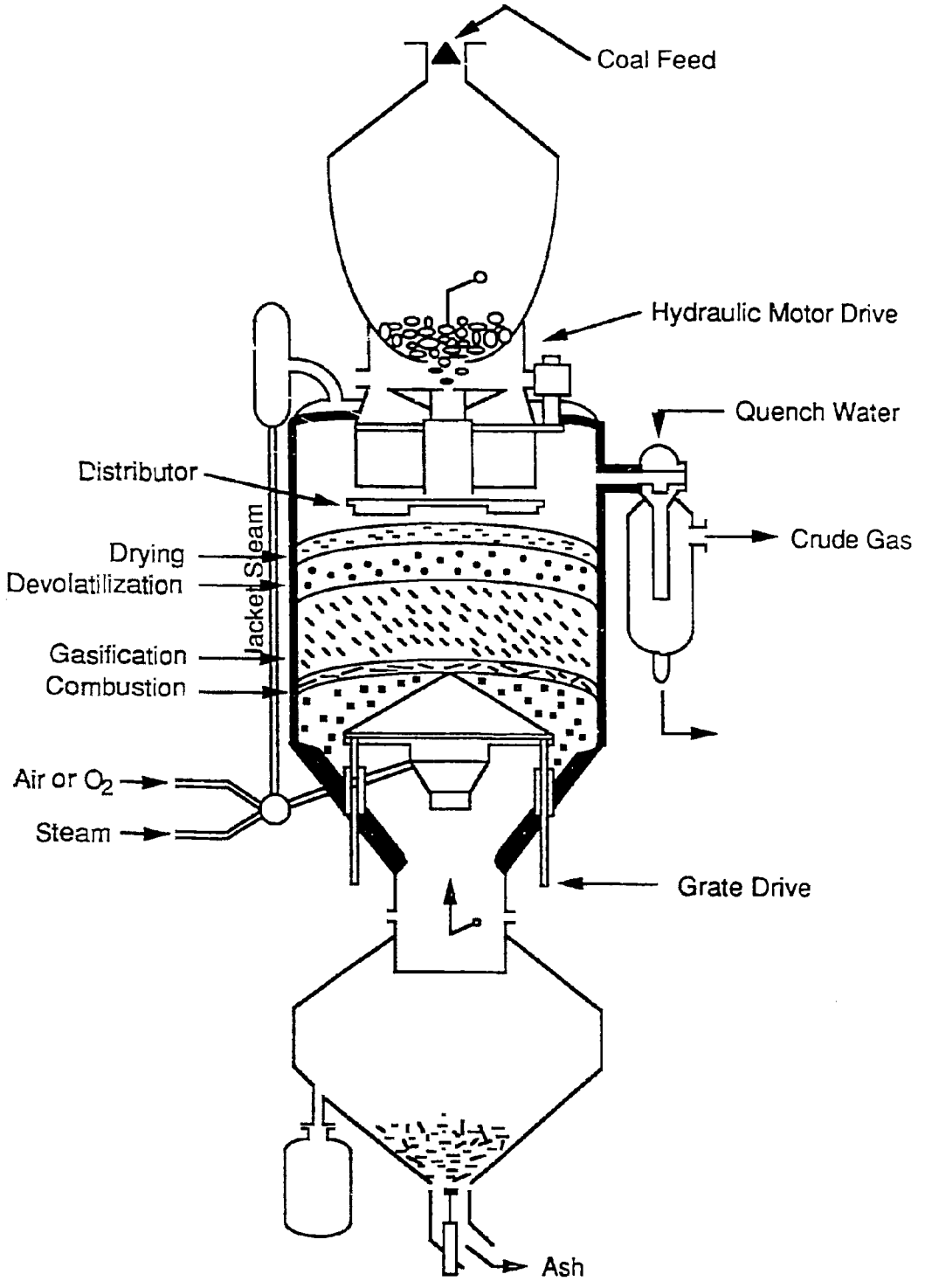


Figure III.B-7. Idealized zones of a typical fixed-bed coal gasifier.

assumed for the improved fixed-bed model. The particle submodel for this zone does not include all the details of heat and mass transfer; it is based on a two-step model of Kobayashi, et al. (1977), and Ubhayakar, et al. (1977). Devolatilization is assumed thermally neutral. A detailed devolatilization submodel (i.e. FG/DVC) will be included in the advanced model.

The residual char is assumed to be pure carbon; hydrogen, oxygen, nitrogen, and sulfur in coal are released during devolatilization. The char combustion and gasification processes are then modeled with various rate expressions. The gasification processes are modeled by the volumetric reaction model; all are assumed reversible. The combustion process is modeled by the shrinking core model; it is assumed irreversible. The gas in reactor is assumed to consist of CO, $CO_2$, $H_2O$, $H_2S$, $N_2$ (including Ar), and $CH_4$. The gasifier pressure is assumed constant.

**Governing Equations and Boundary Conditions** - The differential equation set for the improved moving-bed model is shown in Table III.B-3. The auxiliary equations are shown in Table III.B-4. The boundary conditions necessary to solve Equations III.B-13 through 19 are as follows:

1. Symmetry of the bed with respect to the centerline:

$$\text{at} \quad r=0 \qquad \frac{\partial w_i}{\partial r}=0, \quad \frac{\partial T_s}{\partial r}=0, \quad \frac{\partial T_a}{\partial r}=0 \tag{III.B-24}$$

2. No penetration of mass through the wall:

$$\text{at} \quad r=R \qquad \frac{\partial w_i}{\partial r}=0 \tag{III.B-25}$$

3. No heat accumulation at the wall:

$$\text{at} \quad r=R \qquad K_{gr}\frac{\partial T_g}{\partial r}=h_{wg}(T_{g,b}-T_w), \quad K_{sr}\frac{\partial T_s}{\partial r}=h_{ws}(T_{s,b}-T_w) \tag{III.B-26}$$

The temperature of water inside the water jacket, $T_w$, is taken to be constant at 490 K. This is the saturation temperature of steam at system pressure.

4. The operating input conditions:

$$\text{at} \quad z=0, \qquad w_i=w_i^o(r,0,t), T_g=T_g^o(r,0,t), \; v_g=v_g^o(r,0,t) \tag{III.B-27}$$

$$\text{at} \quad z=L, \qquad y_k=y_k^o(r,L,t), \; T_s=T_s^o(r,L,t) \tag{III.B-28}$$

Table III.B-3. Summary of Model Differential Equations for Improved Fixed-Bed Model

| Eq. No. | Type | Equation |
|---|---|---|
| (III.B-13) | Gas species mass balance | $\frac{\partial w_i}{\partial t} = -v_g \frac{\partial w_i}{\partial z} + \frac{1}{r}\frac{\partial}{\partial r}\left(rD^i_{eff}\frac{\partial w_i}{\partial r}\right) + \frac{1}{\phi\rho_g}(S_{g,i} - w_i S_T)$ |
| (III.B-14) | Total gas mass balance | $\frac{\partial \rho_g}{\partial t} = -\frac{\partial (v_g \rho_g)}{\partial z} + \frac{S_T}{\phi}$ |
| (III.B-15) | Total gas energy balance | $\frac{\partial T_g}{\partial t} = -v_g\frac{\partial T_g}{\partial z} - \frac{1}{C_{pg}}\left[\sum_j h^o_{g,j}\left(\frac{\partial w_j}{\partial t} + v_g\frac{\partial w_j}{\partial z}\right)\right] + \frac{1}{\phi\rho_g C_{pg}}\left[\frac{1}{r}\frac{\partial}{\partial r}\left(r\phi K_{gr}\frac{\partial T_g}{\partial r}\right) + Q_T + \sum_j S_{g,j}h_{g,j} - h_g S_T\right]$ |
| (III.B-16) | Solid species mass balance | $\frac{\partial y_i}{\partial t} = v_s\frac{\partial y_i}{\partial z} + \frac{(S_{c,i} - w_i S_T)}{(1-\phi)\rho_c}$ |
| (III.B-17) | Total solid mass balance | $\frac{\partial \rho_c}{\partial t} = v_s\frac{\partial \rho_c}{\partial z} + \frac{S_T}{(1-\phi)}$ |
| (III.B-18) | Total solid energy balance | $\frac{\partial T_s}{\partial t} = v_s\frac{\partial T_s}{\partial z} + \frac{1}{(1-\phi)\rho_c C_{pc}}\frac{1}{r}\frac{\partial}{\partial r}\left(r(1-\phi)K_{sr}\frac{\partial T_s}{\partial r}\right) + \frac{1}{(1-\phi)}\left(-Q_T - \sum_j S_{s,j}h_{g,j}\right)$ |
| (III.B-19) | Gas momentum equation | $\frac{\partial v_g}{\partial z} = \frac{\sum_j \frac{1}{M_j}\left(\frac{\partial w_j}{\partial t} + v_g\frac{\partial w_j}{\partial z}\right)}{\sum_j\left(\frac{w_j}{M_j}\right)} + \frac{1}{T_g}\left(\frac{\partial T_g}{\partial t} + v_g\frac{\partial T_g}{\partial z}\right) + \frac{S_T}{\phi\rho_g}$ |

Table III.B-4. Auxilliary Equations for Improved Fixed-Bed Model

| Eq. No. | Type | Equation |
|---|---|---|
| (III.B-20) | Heat transfer between solid and gas phases | $Q_T = h_p \frac{6(1-\phi)}{d_p} (T_s - T_g)$ |
| (III.B-21) | Ideal gas law | $\frac{p}{R} = \rho_g T_g \sum_j (\frac{w_j}{M_j})$ |
| (III.B-22) | Total gas phase enthalpy | $h_g = \sum_j w_j h^o_{g,j} + \int_{T_o}^{T_g} C_{pg} dT$ |
| (III.B-23) | Total gas phase production | $S_T = \sum_i S_{s,i}$ |

5. The initial conditions:

$$\text{at } t=0, \quad T_g = T_g^o(r,z,0),\ T_s = T_s^o(r,z,0),\ w_i = w_i^o(r,z,0),$$
$$y_k = y_k^o(r,z,0) \qquad \text{(III.B-29)}$$

The input properties, model parameters, dependent and independent variables are summarized in Table III.B-5.

**Submodel Equations** - The important reactions considered in the improved moving-bed model are shown in Table III.B-6. The gasification reactions R1, R2, and R3 are considered reversible. The equilibrium constants for the reactions follow an Arrhenius form:

$$K_i = K_i^o \exp\left(-\frac{\Delta H_i^o}{RT_g}\right) \qquad \text{(III.B-30)}$$

The intrinsic reaction rates of reactions Ri through R5 are assumed to follow the mass action law, and the rate constants have Arrhenius form:

$$k_{r,i} = k_{i,o} \exp\left(-\frac{E_i}{RT_g}\right) \qquad \text{(III.B-31)}$$

The kinetic parameters depend upon the specific type of coal used. An Illinois No. 6 bituminous coal has comparatively low reactivity while a Wyoming subbituminous coal has comparatively high reactivity. The kinetic and equilibrium parameters for these two coals are listed in Tables III.B-7 and 8. In the char-oxygen reaction, the main difficulty is in predicting the molar ratio of CO to $CO_2$ produced. In this work, a relation of the form

$$\frac{CO}{CO_2} = k \exp\left(-\frac{E}{RT_g}\right) \qquad \text{(III.B-32)}$$

proposed by Rossberg (1956) is used.

**Numerical Solution and Computer Program** - The computer code consists of the main program, 17 original subroutines, and one library subroutine with two user-supplied subroutines. The structure of the computer program is shown in Figure III.B-8, and the functions of the subroutines are listed in Table III.B-9.

The split boundary value problem resulting from the mass and energy balances for countercurrent flow may be solved by several methods. The simplest approach is to use a shooting method in which equations are integrated from the bottom to the top using a marching-type integration method. While this method worked well for the homogeneous case (Yoon et al., 1978), it was disastrous for the heterogeneous model. Amundson and Arri (1978) also reported similar difficulties. In an attempt to overcome this difficulty, a dynamic model was suggested. The system of simultaneous partial differential equations thus has three dimensions: axial position, radial position, and time, and each dimension must be treated separately. For the improved model, orthogonal collocation is used for radial dimension, with finite differencing in the time domain

Table III.B-5. Model parameters and variables

Input Data

| | |
|---|---|
| Gas velocity ($v_g$) | Solid Velocity ($v_s$) |
| Gas composition ($w_i$) | Solid species composition ($y_k$) |
| Gas temperature ($T_g$) | Solid temperature ($T_s$) |
| Pressure (P) | Wall temperature ($T_w$) |

Reactor Parameters

| | |
|---|---|
| Dimensions (diameter, length) | Operating conditions |

Independent Variables

| | |
|---|---|
| Physical coordinates (r, z) | time (t) |

Dependent Variables

| | |
|---|---|
| Gas velocity ($v_g$) | Gas composition ($w_i$) |
| Gas temperature ($T_g$) | Solid temperature ($T_s$) |
| Pressure (P) | Wall temperature ($T_w$) |
| Extent of reaction ($S_{s,i}$, $S_T$) | Solid species composition ($y_k$) |

Table III.B-6. Major reactions occurring in the gasifier[a]

| | |
|---|---|
| $C + H_2O \rightarrow CO + H_2$ | (R1) |
| $C + CO_2 \rightarrow 2CO$ | (R2) |
| $C + 2H_2 \rightarrow CH_4$ | (R3) |
| $C + kO_2 \rightarrow (2\text{-}2k)CO + (2k\text{-}1)CO_2$ | (R4) |
| $C + H_2O \rightarrow CO_2 + H_2$ | (R5) |

[a]Gasification, reactions 1-3. Combustion, reaction 4. Water-gas shift, reaction 5.

Table III.B-7. Reaction Parameters for Illinois and Wyoming Coal

| Reaction | $k^o_{r,i}$ (kPa hr) | $E_i \times 10^{-5}$ (kJ/kmol) | Reference |
|---|---|---|---|
| R1 | | | |
| Illinois | $2.178 \times 10^4$ | 1.757 | Cho (1980) |
| Wyoming | $1.464 \times 10^4$ | 1.465 | Yoon et al. (1978) |
| R3 | | | |
| Illinois | $1.465 \times 10^{-4}$ | 0.6716 | * |
| Wyoming | $2.931 \times 10^{-4}$ | 0.6716 | Cho (1980) |
| R4 | | | |
| Illinois | $6.360 \times 10^7$ | 1.13 | Cho (1980) |
| Wyoming | $6.360 \times 10^7$ | 1.13 | Cho (1980) |

* "No data are available in the literature"
$k^o_r$ is assumed as one half of that of Wyoming coal
$k_{r,co2}$ was assumed as 0.6 $k_{r,H2O}$ (Yoon et al., 1978)

Table III.B-8. Equilibrium parameters

| | Equilibrium Parameters | | |
|---|---|---|---|
| Reaction | $K^o_i$ | $\Delta H^o_i$(kcal/mole) | Reference |
| R1 | $3.098 \times 10^7$ | 32.457 | Yoon et al. (1978) |
| R2 | $1.222 \times 10^9$ | 40.300 | Yoon et al. (1978) |
| R3 | $1.472 \times 10^{-5}$ | -21.854 | Yoon et al. (1978) |
| R4 | infinite (irreversible) | | |
| R5 | 0.0265 | -7.860 | Yoon et al. (1978) |

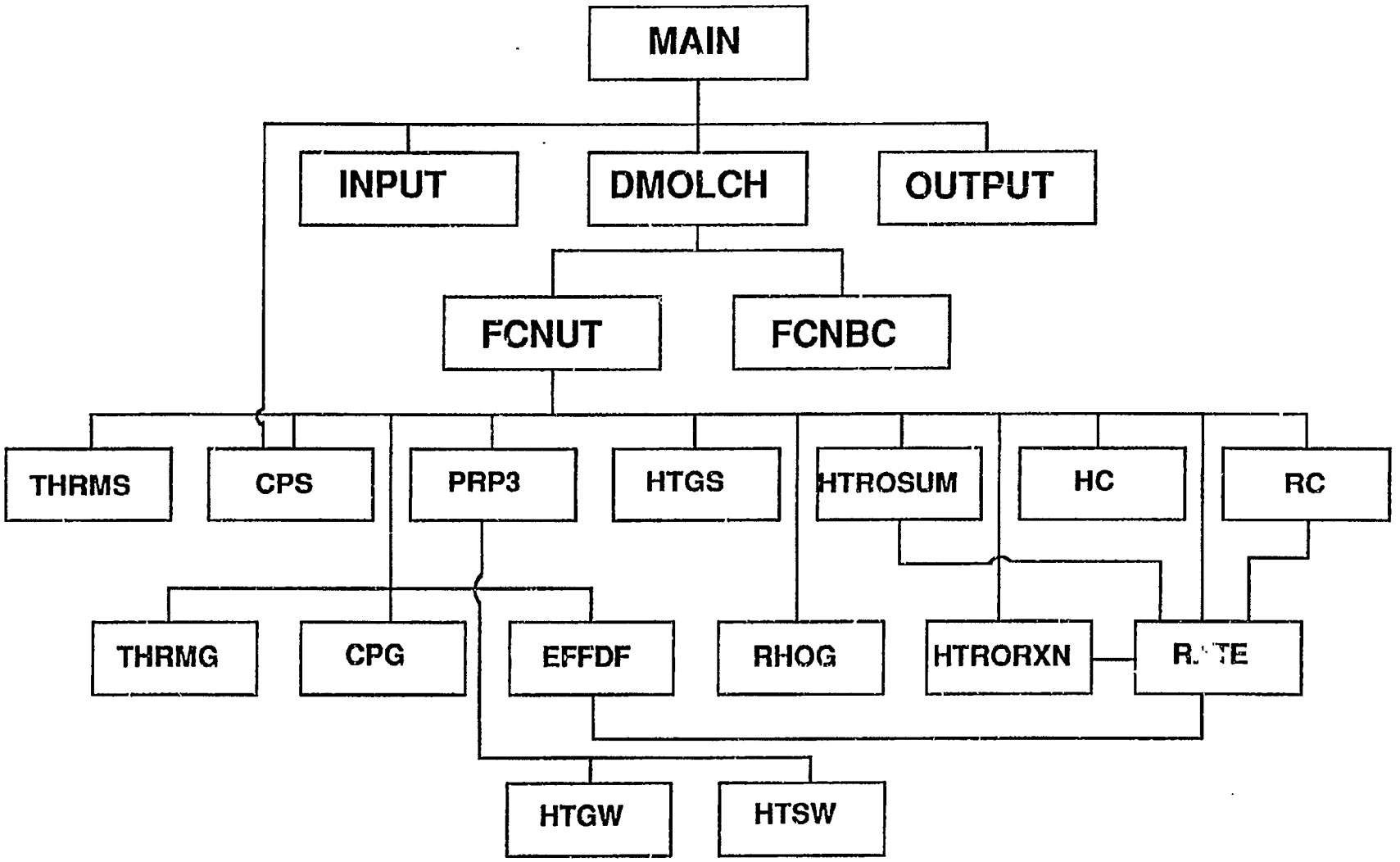


Figure III.B-3 Improved fixed-bed program structure.

Table III.B-9. List of Subroutines

| Subroutine | Function | Controlling Program | Input to Subroutine | Output from Subroutine |
|---|---|---|---|---|
| INPUT | to read and print input data | MAIN program | all input data except data given by data statements | same as left |
| OUTPUT | to print output data | MAIN | all output data | - |
| THRMS | to calculate effective solid phase thermal conductivity | FCNUT | solid temperature conductivity | effective solid thermal |
| CPS | to calculate heat capacity of char | FCNUT | solid temperature | heat capacity of coal |
| PRP3 | to calculate boundary conditions at the wall of the gasifier for both mass and energy conservation equations | FCNUT | gas temperature solid temperature gas compositions | boundary condition at the wall of the gasifier |
| HTGS | to calculate gas-solid heat transfer coefficient | FCNUT | solid temperature, gas compositions | gas-solid heat transfer coefficient |
| HTROSUM | to calculate summation of enthalpy production due to heterogeneous reaction | FCNUT | solid temperature, gas temperature, gas compositions | summation of enthalpy production due to heterogeneous reaction |
| HC | to calculate enthalpy of coal | FCNUT | solid temperature | enthalpy of coal |
| RC | to calculate carbon reaction rate | FCNUT | solid temperature | carbon reaction rate |
| THRMG | to calculate effective gas phase thermal conductivity | FCNUT | gas temperature conductivity | effective gas thermal conductivity |
| CPG | to calculate heat | FCNUT | gas temperature, | heat capacity of gas |

Table III.B-9. List of Subroutines (continued)

| Subroutine | Function | Controlling Program | Input to Subroutine | Output from Subroutine |
|---|---|---|---|---|
| | capacity of gas mixture | | gas compositions | mixture |
| EFFDF | to calculate effective radial diffusivity of gas phase | FCNUT | gas temperature diffusivity | effective gas radial diffusivity |
| RHOG | to calculate total density of gas | FCNUT | gas temperature, gas compositions | total gas density |
| HTRORXN | to calculate summation of reaction rate of heterogeneous reaction | FCNUT | solid temperature, gas compositions | summation of reaction rate of heterogeneous reaction |
| RATE | to calculate reaction rate of heterogeneous reaction | FCNUT | solid temperature, gas compositions | reaction rate of heterogeneous reaction |
| HTGW | to calculate gas-wall heat transfer coefficient | FCNUT | gas temperature coefficient | gas-wall heat transfer coefficient |
| HTSW | to calculate solid-wall heat transfer coefficient | FCNUT | solid temperature | solid-wall heat transfer coefficient |
| DMOLCH | to integrate parabolic partial differential equations by the method of line approach | MAIN | developed by IMSL | |
| FCNUT | to transform PDE's into ODE's | MAIN (DMOLCH) | developed by IMSL | |
| FCNBC | to provide boundary conditions | MAIN (DMOLCH) | developed by IMSL | |

(Bhattacharya et al., 1986). Thus, the set of the PDE's can be rewritten as a larger set of ODE's in the axial direction. This set of equations was numerically integrated using, first, an IMSL routine IVPG based on Gear's method (Gear, 1971). However, this method did not work; the split boundary conditions seemed to be the cause of the difficulties. To avoid this, another IMSL routine, MOLCH, was tried; this routine is based on the method of lines. The differential equations were first discretized in radial direction using three collocation points. Since a symmetrical trial function was used to generate orthogonal polynomials, the boundary condition at the center of the gasifier was automatically satisfied. For the boundary condition at the wall of the gasifier, the third collocation point was used. This way, 11 parabolic partial differential equations in radial and axial dimensions were cast into 22 parabolic partial differential equations in axial dimension. DMOLCH uses a cubic Hermite collocation method for spatial discretization; 10 collocation points in axial dimension result in 220 simultaneous initial value problems. They have a bandwidth matrix of 440 with 130 elements. These equations are integrated in time by DGEAR. It is estimated that to reach a steady-state solution, at least 30 hours would be required. Besides, DGEAR does not take advantage of the sparsity of the matrix. Therefore, very substantial computer time will be required to solve this set of equations.

The improved fixed-bed model status is as follows: The model assumptions have been determined and the model formulated. The governing equations, boundary conditions, and auxiliary equations have been developed. The submodel equations have been selected. The numerical method has been selected and the computer program coded. The existing submodels for large-particle devolatilization and heterogeneous reactions, solid and gas flow, and numerical methods have been found inadequate. The computer program execution times have been found excessive. The improved fixed-bed model has provided a basis for the advanced fixed-bed model development. Further work on the improved fixed-bed model will be at a low level of effort. The major thrust will be on the advanced model.

Advanced Fixed-Bed Model - Based on experiences with the improved fixed bed model, work has been initiated on the advanced fixed bed model. Key model assumptions are listed in Table III.B-10. Due to the presence of radial temperature and, presumably, concentration gradients, the advanced code is to be 2-dimensional. Devolatilization and other solids reaction processes will be generalized using the large particle submodel being developed under Subtask 2.e. Due to the finite rate of heat transfer between solids and gas, and the importance of predicting solids temperature accurately for the detailed particle submodel, gas and solids temperatures will be allowed to vary independently. Extension of the gas-phase reactions to include a wider variety of species will be considered assuming thermodynamic equilibrium. Frozen equilibrium on chemical kinetics may be required for liquid products important in mild gasification. Formation and destruction of pollutant species may also be considered, based on the submodel for the entrained-bed code being developed under Subtask 2.g. Solids flow is a particularly critical issue in fixed-bed modeling. Assumption of plug flow is considered to be inadequate. Relating irregular solids flow to coal conversion (Thorsness and Kang, 1986) is viewed as a reasonable starting point.

## TABLE III.B-10

## KEY MODEL ASSUMPTIONS

### General

- Two-dimensional, axisymmetric, counterflow
- Separate gas and solids temperatures
- Transient or steady-state
- Radiation by diffusion approximation

### Gas Phase

- Ideal gas
- Radial diffusion/conduction by effective bed coefficients
- Pressure drop by Ergun equation (Ergun, 1952)
- Laminar, continuum
- Partial equilibrium
- No axial diffusion or conduction
- Sulfur species in equilibrium
- $NO_x$ species in non-equilibrium

### Solid Phase

- No radial dispersion of solids
- Large particle temperature gradient effects related to coal conversion
- Bed-settling (Thorsness and Kang, 1986)
- No particle agglomeration
- Duel reaction steps (devolatilization, char oxidation)
- Decoupled devolatilization zone
- Multiple oxidizers ($O_2$, $CO_2$, $H_2O$)
- Neglect particle fragmentation
- Multiple particle sizes and/or types

**Governing Equations and Boundary Conditions** - The preliminary forms of the general governing equations for the advanced fixed-bed model were given in the First Annual Report (Solomon et al., 1987) and in the Fixed-Bed Research Plan (Smoot et al., 1987). These equations have been rederived based on the derivations of Crowe (1976) and Smoot (1979), extended to dense-phase systems. The equations are similar to those of the improved fixed-bed model, but are being developed for a different set of assumptions. The equations and assumptions will be documented in a future report.

**Submodel Equations** - The flow of solids is a particularly critical issue in fixed-bed modeling. All known attempts to develop a model for predicting the behavior of bulk solids during flow have been based on either the particulate or the continuum approach. The continuum approach, based on the work of Jenike and Johansen (1976, 1972), has been proven in engineering practice. Thus, it was selected for further consideration.

## Plans

The collection of the fixed-bed design and test data as well as work on the comprehensive review of fixed-bed combustion and gasification will be continued. Little additional work will be conducted on the improved fixed-bed model, as its assumptions are somewhat restrictive. Emphasis will be on the advanced model, suitable for incorporating the advanced submodels being developed under Subtasks 2.e and 2.f. The governing equations and the boundary conditions will be finalized. Particular attention will be paid to the flow of solids and the radiation heat transfer. The submodels for these processes will be developed. Based on a literature review and recommendations of expert consultants, a numerical method appropriate for the advanced fixed-bed model will be selected. The computer code will be developed and initial debugging, testing, and validation will be performed. Integration of the advanced submodels, particularly the large particle submodel developed under Subtask 2.e, will be initiated.

## Nomenclature

| | |
|---|---|
| $[CO]$ | Molar concentration of carbon monoxide [mol/$m^3$] |
| $[CO_2]$ | Molar concentration of carbon dioxide [mol/$m^3$] |
| $C_p$ | local gas heat capacity [kJ/kmol K] |
| $C_{pg}$ | total gas phase heat capacity [kJ/kmol K] |
| $C_{pc}$ | total solid phase heat capacity [kJ/kmol K] |
| $D_{ieff}$ | effective radial diffusivity of species i [$m^2$/hr] |
| $D_f$ | diameter of the reactor [m] |
| $D_{ea}$ | effective axial diffusivity [$m^2$/hr] |
| $D_{er}$ | effective radial diffusivity [$m^2$/hr] |
| $d_p$ | particle diameter [m] |
| $E_i$ | activation of energy of reaction i [kJ/kgmol] |
| $F_G$ | total molar flux of gas stream [kmol/$m^2$ hr] |
| f | pressure drop |
| f | proportionality factor for the gas-solid heat transfer coefficient of the coal bed |
| G | mass flux of the gas stream [kg/$m^2$ hr] |
| $h_p$ | gas-solid heat transfer coefficient of the coal bed [kJ/$m^2$ hr K] |
| $h_{rw}$ | heat transfer coefficient for thermal radiation, void space to void space [kJ/$m^2$ hr K] |
| $h_{rs}$ | equivalent radiation heat transfer coefficient for the solid phase [kJ/$m^2$ hr K] |
| $h_w$ | homogeneous bed-to-wall effective heat transfer coefficient [kJ/$m^2$ hr K] |
| $h_{gw}$ | effective wall heat transfer coefficient for gas phase [kJ/$m^2$ hr K] |
| $h_{sw}$ | effective wall heat transfer coefficient for solid phase [kJ/$m^2$ hr K] |
| hg | total enthalpy of gas phase [kJ/kgmol] |
| $h_{g,j}$ | enthalpy of gas species j [kJ/kgmol] |
| $h_p$ | particle-to-particle contact heat transfer coefficient [kJ/$m^2$ hr K] |
| $K_a$ | effective axial thermal conductivity [kJ/hr m K] |
| $K_{sea}$ | static contribution of effective radial thermal conductivity [kJ/hr m K] |
| $K_{gsea}$ | static contribution of effective axial gas thermal conductivity [kJ/hr m K] |
| $K_g$ | gas thermal conductivity [kJ/hr m K] |
| $K_{gr}$ | effective radial gas conductivity [kJ/hr m K] |
| $K_{sr}$ | effective radial solid conductivity [kJ/hr m K] |
| $K_s$ | solid thermal conductivity [kJ/hr m K] |
| k | pre-exponential factor |
| $k_{r,i}$ | intrinsic reaction rate of species i [kmol/kmol char kPa hr] |
| $k_{or,i}$ | Arrhenius constant for intrinsic reaction rate of species i [kmol/kmol char kPa hr] |
| $K_i$ | equilibrium constant of reaction i |
| $K_{oi}$ | pre-exponential factor in equilibrium constant of reaction i |
| $k_{g,i}$ | mass transfer coefficient of gaseous species i through bulk film |
| L | reactor length [m] |
| $M_j$ | molecular weight of species j [kg/kgmol] |
| $M_w$ | mixture molecular weight of species [kg/kgmol] |
| P | total pressure [kPa] |
| $P_e$ | Peclet number |
| $P_i$ | partial pressure of gas species i [kPa] |
| $P_{fa,i}$ | film pressure factor of species i |

| | |
|---|---|
| $P_r$ | Prandtl number |
| $Q_T$ | heat transfer between gas and solid phase [kJ/m$^3$ hr] |
| r | radial direction [m] |
| R | reactor radius [m] |
| R | universal gas constant |
| $R_e$ | Reynolds number |
| $S_c$ | total solid phase source per volume of bed [kg/m$^3$ hr] |
| $S_{c,k}$ | solid species k source per volume of bed [kg/m$^3$ hr] |
| $S_{s,i}$ | species i gas source per volume of bed by heterogeneous reaction [kg/m$^3$ hr] |
| $S_T$ | total gas phase source per volume of bed [kg/m$^3$ hr] |
| $T_g$ | gas phase temperature [K] |
| $T_s$ | solid phase temperature [K] |
| $T_w$ | wall temperature [K] |
| t | time, [hr] |
| $U_g$ | superficial gas velocity [m/hr] |
| $U_{g,a}$ | superficial axial gas velocity [m/hr] |
| $U_{g,r}$ | superficial radial gas velocity [m/hr] |
| $v_g$ | interstitial gas velocity [m/hr] |
| $v_s$ | effective solid velocity [m/hr] |
| $w_i$ | weight fraction of gas species i |
| $y_k$ | weight fraction of solid species k |
| z | axial direction [m] |

Greek symbols

| | |
|---|---|
| $\beta$ | effective length between centers of neighboring solid particles divided by equivalent diameter of the particles |
| $\chi$ | effective thickness of the fluid film adjacent to the surface of two solid particles divided by equivalent diameter of the particles |
| $\delta_1$ | parameter in effective axial conductivity |
| $\delta_2$ | parameter in effective axial conductivity |
| $\gamma$ | effective length of a clogged particle for heat transfer divided by the equivalent diameter of the particle |
| $\epsilon$ | emissivity of the solid |
| $\phi$ | bed porosity |
| $\rho_c$ | total solid density [kg/m$^3$] |
| $\rho_g$ | total gas density [kg/m$^3$] |
| $\varnothing$ | total bed porosity |

Superscripts

| | |
|---|---|
| o | Initial condition |